

Extragalactic astrophysics with next-generation CMB experiments

G. De Zotti^{1,*}, M. Bonato^{2,3,1}, M. Negrello⁴, T. Trombetti², C. Burigana^{2,5,6}, D. Herranz^{7,8}, M. López-Caniego⁹, Z.-Y. Cai¹⁰, L. Bonavera¹¹ and J. González-Nuevo¹¹

¹INAF, Osservatorio Astronomico di Padova, Vicolo dell'Osservatorio 5, I-35122 Padova, Italy

²INAF, Istituto di Radioastronomia, Via Piero Gobetti 101, I-40129 Bologna, Italy

³INAF, Italian ALMA Regional Centre, Via Gobetti 101, I-40129, Bologna, Italy

⁴School of Physics and Astronomy, Cardiff University, The Parade, Cardiff CF24 3AA, UK

⁵Dipartimento di Fisica e Scienze della Terra, Università di Ferrara, Via Giuseppe Saragat 1, I-44122 Ferrara, Italy

⁶INFN, Sezione di Bologna, Via Irnerio 46, I-40127 Bologna, Italy

⁷Instituto de Física de Cantabria, CSIC-UC, Av. de Los Castros s/n, E-39005 Santander, Spain

⁸Departamento de Física Moderna, Universidad de Cantabria, 39005-Santander, Spain

⁹ESAC, Camino Bajo del Castillo s/n, Urb. Villafranca del Castillo 28692, Villanueva de la Canada - Madrid, Spain

¹⁰CAS Key Laboratory for Research in Galaxies and Cosmology, Department of Astronomy, University of Science and Technology of China, Hefei, Anhui 230026, China

¹¹Departamento de Física, Universidad de Oviedo, C. Federico García Lorca 18, 33007 Oviedo, Spain

Correspondence*:
Gianfranco De Zotti
gianfranco.dezotti@inaf.it

ABSTRACT

Planck, SPT and ACT surveys have clearly demonstrated that Cosmic Microwave Background (CMB) experiments, while optimised for cosmological measurements, have made important contributions to the field of extragalactic astrophysics in the last decade. Future CMB experiments have the potential to make even greater contributions. One example is the detection of high- z galaxies with extreme gravitational amplifications. The combination of flux boosting and of stretching of the images has allowed the investigation of the structure of galaxies at $z \simeq 3$ with the astounding spatial resolution of about 60 pc. Another example is the detection of proto-clusters of dusty galaxies at high z when they may not yet possess the hot intergalactic medium allowing their detection in X-rays or via the Sunyaev-Zeldovich effect. Next generation CMB experiments, like PICO, CORE, CMB-Bharat from space and Simons Observatory and CMB-S4 from the ground, will discover several thousands of strongly lensed galaxies out to $z \sim 6$ or more and of

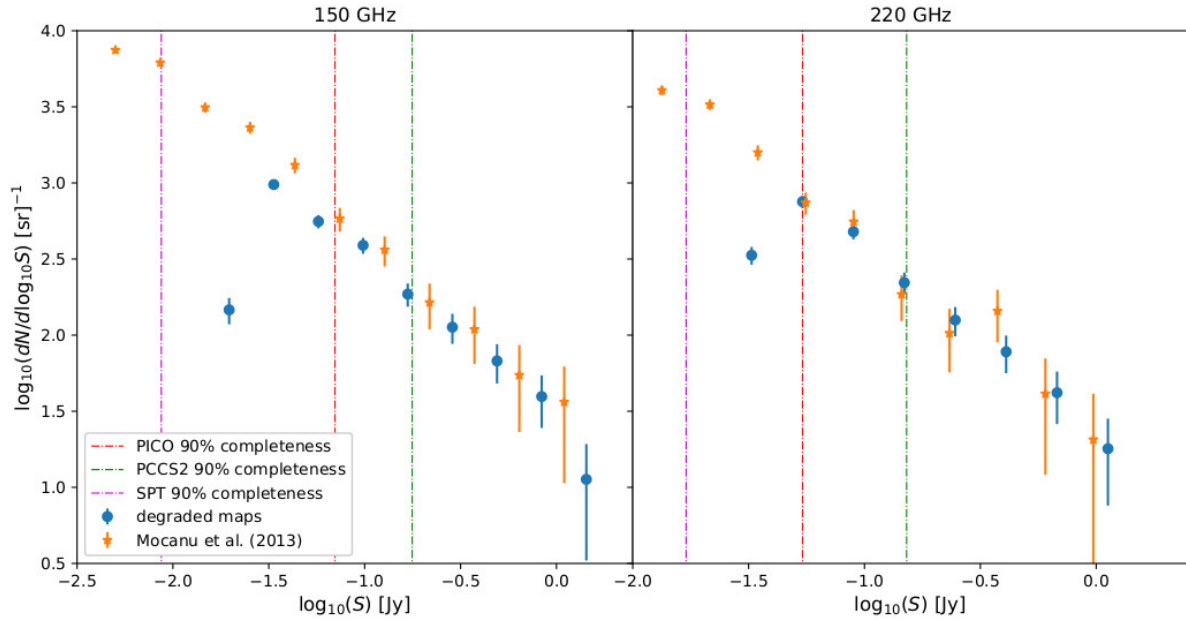


Figure 1. Effect of angular resolution on the confusion limit. The filled blue circles show the differential counts of sources on SPT maps degraded to the PICO resolution at 150 GHz (FWHM = $6.2'$; left panel) and 220 GHz (FWHM = $3.6'$; right panel) compared with the SPT counts of Mocanu et al. [5, orange stars]. The vertical dot-dashed lines correspond, from left to right, to the 90% completeness limits at the full SPT resolution, at the PICO resolution and at the *Planck* resolution.

galaxy proto-clusters caught in the phase when their member galaxies were forming the bulk of their stars. They will also detect tens of thousands of local dusty galaxies and thousands of radio sources at least up to $z \simeq 5$. Moreover they will measure the polarized emission of thousands of radio sources and of dusty galaxies at mm/sub-mm wavelengths.

Keywords: Cosmic Microwave Background, galaxy surveys, radio sources, strong lensing, sub-millimeter galaxies, proto-clusters

1 INTRODUCTION

WMAP and even more *Planck* have already provided an exciting foretaste of the potential of space-borne Cosmic Microwave Background (CMB) experiments for extragalactic astrophysics. Next generation experiments with telescope sizes similar to *Planck*'s, like the Cosmic Origins Explorer [CORE; 1], the Probe of Inflation and Cosmic Origins [PICO; 2] or CMB Bharat¹ can do much better. This is because, for state-of-the-art instruments with sensitivity at fundamental limits (as *Planck* also was) the detection limit is not set by instrumental noise but by fluctuations of astrophysical foregrounds (confusion noise), whose amplitude, at the frequencies and angular scales of interest, is roughly proportional to the beam solid angle [see Fig. 3 of ref. 3]. *Planck* did not work at the diffraction limit while next generation experiments will. The improvement in angular resolution will be substantial. For example, at 545 GHz ($550 \mu\text{m}$) the *Planck* beam has an effective full-width at half maximum FWHM = $4.83'$ [4] while the diffraction limit for its 1.5 m telescope is $1.5'$. Improving the resolution to the diffraction limit decreases the detection limit at this frequency by about one order of magnitude.

¹ <http://cmb-bharat.in/>

The De Zotti et al. [3] results on the impact of angular resolution on the detection limits, based on simulations exploiting the *Planck* sky model [6], have been improved using real data. To this end we degraded the publicly available South Pole Telescope (SPT) maps of 2540 deg^2 at 95, 150 and 220 GHz [7], with resolutions of approximately $1.7'$, $1.2'$, and $1.0'$, respectively, to the PICO resolution (FWHM = $9.5'$, $6.2'$ and $3.6'$, respectively) and applied to the degraded maps the Mexican Hat Wavelet 2 (MHW2) source detections algorithm [8, 9], also used to build the Second *Planck* Catalogue of Compact Sources [PCCS2; 10]. The results at 150 and 220 GHz are illustrated by Fig. 1. The completeness limits for the degraded maps were obtained by comparison with the SPT counts. We found 90% completeness down to 95, 70 and 55 mJy at 95, 150 and 220 GHz, respectively. For comparison, the PCCS2 90% completeness limits² in the “extragalactic zone” are 269, 177 and 142 mJy, respectively [4]. The PICO detection limits at the other frequencies were obtained by means of analytical extrapolations of results obtained from simulations done for the CORE project [11]. These extrapolations were found to be consistent with the determinations based on degraded SPT maps and with the PCCS2 90% completeness limits in the “extragalactic zone”. Similar detection limits hold for CORE and CMB Bharat.

Fluctuations (hence detection limits) at few arcmin resolution are dominated by compact sources too faint to be detected individually. Such source confusion can be reliably determined from the power spectra of the Cosmic Infrared Background (CIB), measured by *Planck* [12, 13] and by *Herschel* [14]. On larger angular scales, however, fluctuations of diffuse emissions (Galactic or CMB) must also be taken into account.

The potential of ground based CMB experiments has been demonstrated by the SPT [5] and by the Atacama Cosmology Telescope [ACT; 20] surveys. With telescopes of the 6–10 m class, these experiments reach arcmin angular resolution at mm wavelengths, with sensitivity at fundamental limits. Next generation experiments, like CMB-S4 [21] and the Simons Observatory [22] will extend the coverage to at least 40% of the sky.

Space-borne experiments like PICO will cover a very broad frequency range, from $\simeq 20$ to $\simeq 800$ GHz, while observations from the ground are only possible, in atmospheric windows, up to $\simeq 300$ GHz. The extragalactic sky in the frequency range of CMB experiments is dominated by two point source populations: blazars (Flat-Spectrum Radio Quasars and BL Lacertae-type sources) and dusty star-forming galaxies. Blazars are powerful radio-loud active galactic nuclei (AGNs) whose relativistic jets are closely aligned with the line of sight. They overbear the number counts at wavelengths longer than about 1 mm while dusty galaxies prevail at shorter wavelengths. This is illustrated by Fig. 2, where the spectral energy distributions (SEDs) of a $z \simeq 2$ blazar and of two dusty galaxies are compared with the estimated detection limits of the PICO project [2] and with the completeness limits of the SPT surveys [5], extrapolated on one side to 40 GHz and on the other side to 270 GHz to cover the frequency range of CMB-S4. The 90% completeness limits of the PCCS2 in the “extragalactic zone” are also shown for comparison.

In this paper we will discuss the expected outcome of planned next generation CMB experiments with regard to strongly gravitationally lensed high- z dusty galaxies (Sect. 2), galaxy proto-clusters (Sect. 3) and radio sources (Sect. 4). In Sect. 5 we deal with counts of the various classes of extragalactic sources in polarization. The main conclusions are summarized in Sect. 6

We adopt a flat Λ CDM cosmology with the latest values of the parameters derived from Planck CMB power spectra: $H_0 = 67.4 \text{ km s}^{-1} \text{ Mpc}^{-1}$ and $\Omega_m = 0.315$ [23].

² Effective FWHM = $9.68'$, $7.30'$ and $5.02'$ at 100, 143 and 217 GHz, respectively; FWHMs of the Gaussians whose solid angle is equivalent to that of the effective beams.

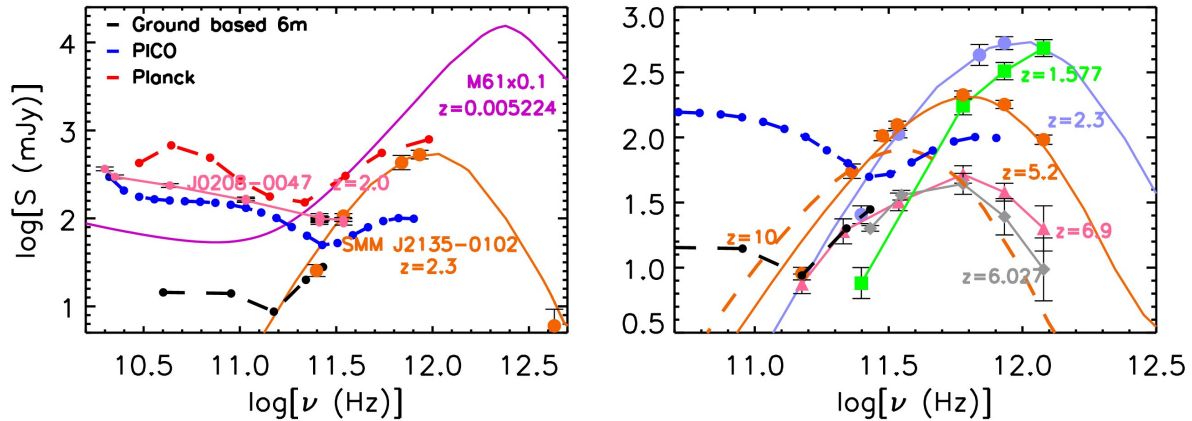


Figure 2. Spectral energy distributions of extragalactic sources in the frequency range of CMB experiments, compared with the estimated detection limits of the PICO project and with the completeness limits of the SPT surveys extrapolated to 40 and to 270 GHz, to cover the range of the CMB-S4 project. The PCCS2 90% completeness limits in the “extragalactic zone” are also shown for comparison (in the left panel only). At wavelengths shorter than a few mm the dominant extragalactic population are dusty star-forming galaxies. At longer wavelengths radio sources, mostly blazars, take over. The spectral energy distributions (SEDs) of blazars are characterized by a relatively flat continuum spectrum exemplified by that of J0208-0047 at $z \simeq 2.0$ (flat solid orange line). Dusty star-forming galaxies are a mixture of local and high- z strongly gravitationally lensed objects. Local galaxies are, by far, the brightest extragalactic sources at sub-mm wavelengths. Their SEDs are exemplified by that of the dusty star-forming galaxy M 61, scaled down by a factor of 10. Some examples of SEDs of strongly lensed galaxies are shown: SDP 9 [$z = 1.577$; 15], SMMJ2135-0102 [$z = 2.3259$; 16], HLS J091828.6+514223 [$z = 5.2$; 17], HATLAS J090045.4+004125 [$z = 6.027$; 18] and SPT-S J031132-5823.4 [$z = 6.9$; 19]. The dashed orange SED represents that of HLS J091828.6+514223 scaled to $z = 10$ to show that galaxies like it are visible up to very high redshifts both by ground-based and by space-borne next generation CMB experiments.

2 DUSTY GALAXIES

2.1 Strongly-lensed galaxies

Next generation CMB experiments will conduct a census of the brightest sub-mm galaxies in the Universe. *Planck*, SPT and ACT have already offered an exciting foretaste of that. Follow-up CO spectroscopy and multi-frequency photometry of 11 “*Planck*’s dusty GEMS” [Gravitationally Enhanced subMillimetre Sources; 30] have shown that they are at $z = 2.2\text{--}3.6$. Their apparent (uncorrected for gravitational amplification) far-IR luminosities are up to $3 \times 10^{14} L_{\odot}$, making them among the brightest sources in the Universe.

Herschel extragalactic surveys yielded a surface density of $\simeq 0.16 \text{ deg}^{-2}$ for $S_{500\mu\text{m}} \geq 100 \text{ mJy}$ [24]. A space-borne 1.5 m telescope will reach a slightly fainter flux density limit over the full sky (excluding the region around the Galactic plane), thus achieving the detection of several thousands of strongly lensed galaxies (upper left-hand panel of Fig. 3). The number of detections decreases rapidly for smaller telescope sizes; a telescope substantially smaller than 1 m cannot do any better than *Planck*. A 2 m telescope would increase the number of strongly lensed detections by a factor $\simeq 2.5$. However their selection would require additional information to distinguish them from unlensed high- z galaxies dominating the counts at the corresponding flux density limit. Efficient methods to separate lensed and unlensed galaxies have been presented by refs. [31, 32].

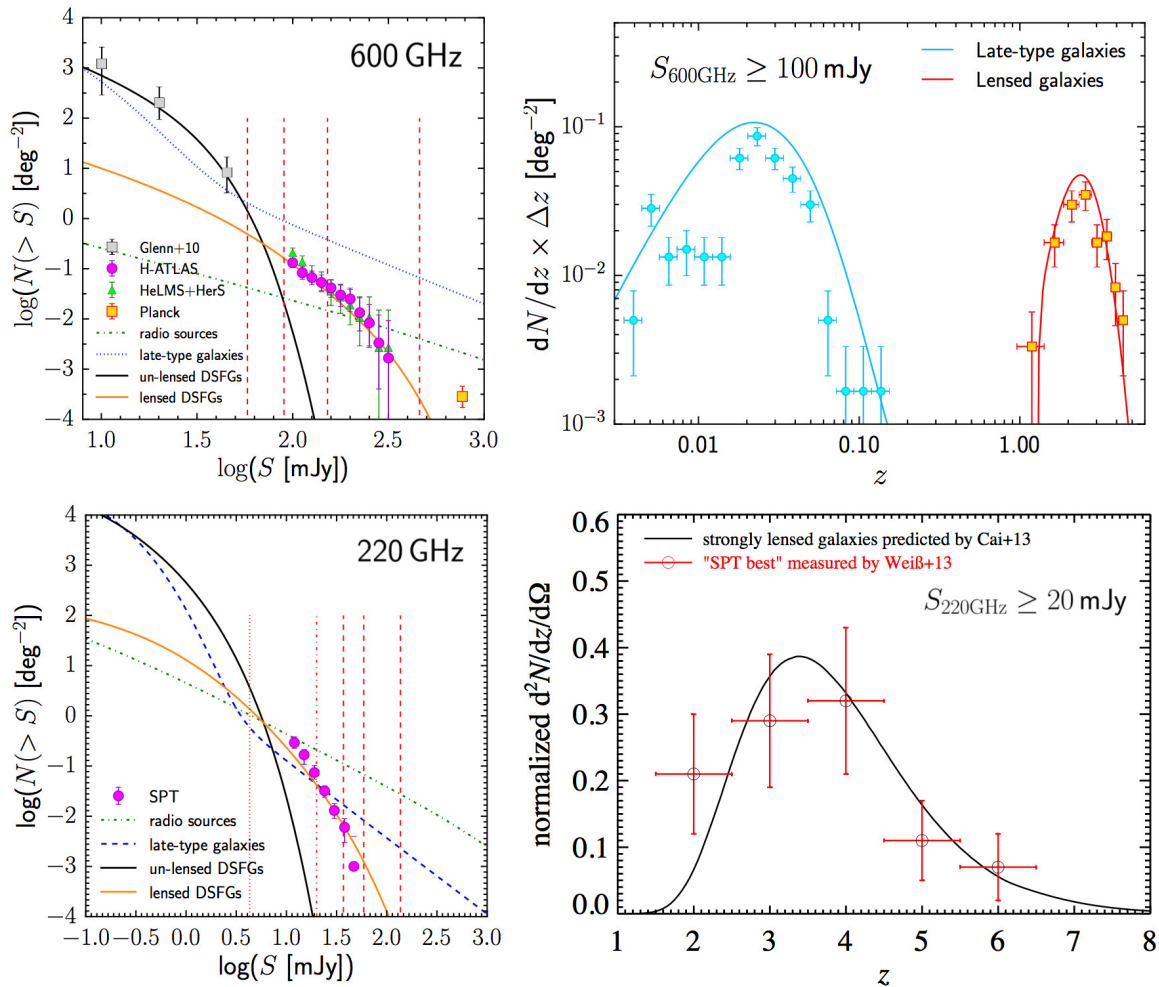


Figure 3. Upper left panel. Integral counts of strongly lensed galaxies from *Herschel* surveys at $500 \mu\text{m}$ [600 GHz; green and magenta data points from ref. [24], compared with the predictions of the Cai et al. [25] model (solid orange line). The yellow square on the bottom-right corner is our own estimate of the counts of strongly lensed galaxies detected by *Planck*. The counts of unlensed proto-spheroidal galaxies (data points from ref. [26], black squares; model by ref. [25], solid black line), of radio sources [dotted green line, model by ref. [27] and of normal and starburst late-type galaxies [dotted blue line, model by ref. [25] are also shown for comparison. The vertical dashed orange lines show, from right to left, the 90% completeness limit of the PCCS2 and the 5σ detection limits for space-borne CMB experiments with 1, 1.5 and 2 m telescopes working at the diffraction limit. This panel shows a modified version of Fig. 8 of Negrello et al. [24]. **Upper right panel.** Redshift distribution of galaxies brighter than 100 mJy at $500 \mu\text{m}$, derived from the full H-ATLAS catalogue (data points with Poisson errors) compared with the predictions of the Cai et al. [25] model (solid lines). There is a clear bimodality. On one side we have nearby late-type galaxies, almost all at $z \leq 0.06$, and hence easily recognizable in optical/near-infrared catalogues. On the other side we have dust enshrouded, hence optically very faint, gravitationally lensed galaxies at $z \geq 1$ and up to $z > 4$. **Lower left panel.** Integral counts of strongly lensed galaxies from the SPT survey at 220 GHz [1.4 mm; magenta data points; 28] compared with the prediction of the Cai et al. [25, orange solid line] model. Counts of radio sources and of late-type galaxies are from the same models as in the upper panel. The vertical lines show, from right to left, the 5σ detection limits for diffraction limited 1, 1.5 and 2 m telescopes, the completeness limit of the SPT survey [5] and the 5σ confusion limit for a 6 m telescope. **Lower right panel.** Estimated redshift distribution of strongly lensed galaxies with $S_{220\text{GHz}} > 20 \text{ mJy}$ [29] compared with the prediction of the Cai et al. [25] model.

Ground-based instruments typically have higher resolution at the longer wavelengths, and thus select a higher redshift population. A straightforward extrapolation of results from analyses in the first [28] and

second [5] SPT catalogue papers imply that the SPT has detected hundreds of strongly lensed galaxies over the full survey area (lower left-hand panel of Fig. 3). Their redshift distribution [29, 33] is broader than found for *Herschel* surveys [24] and the mean redshift, $\bar{z} = 3.5$ [29] is higher (lower right-hand panel of Fig. 3). The maximum spectroscopically measured redshift, $z = 6.9$ [19], shows that this survey has reached the epoch of reionization. Additional samples of strongly lensed galaxies, over a similar redshift range have been provided by the ACT surveys [20, 34].

Next-generation ground-based experiments, extending the sky coverage up to 40% of the sky or more, will detect thousands of strongly lensed galaxies if their performances will be similar to those of the SPT. If these experiments will be able to reach the confusion limit of a 6 m telescope operating at the diffraction limit (4-5 mJy), the number of strongly-lensed detections will increase to tens of thousands.

The right-hand panel of Fig. 2 shows that both ground-based and space-borne experiments will detect strongly lensed galaxies up to high redshifts. For example objects like the strongly lensed galaxy HLS J091828.6+514223 at $z = 5.2$ would be detectable up to z of at least 10 (dashed SED in Fig. 2). Ground-based and space-borne experiments cover complementary redshift ranges. The former are more efficient at $z \gtrsim 2$, the latter at lower z .

These surveys will also probe a large fraction of the entire Hubble volume for the most intense hyper-luminous starbursts, testing whether there are physical limits to the star-formation rates (SFRs) of galaxies [e.g., ref. 35].

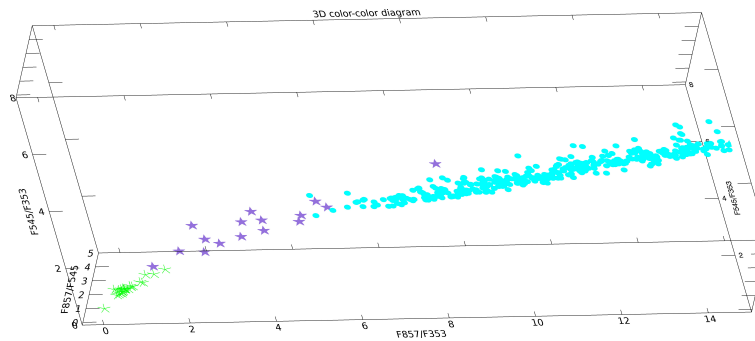


Figure 4. 3D colour-colour plot showing the colours of strongly-lensed galaxies detected by *Planck* (purple stars) compared to those of local galaxies (light blue symbols) and of radio sources (green symbols). The distribution of local galaxies extends to the blue far beyond the chosen boundaries of the figure. Strongly lensed galaxies populate a region intermediate between those of local galaxies and radio sources and well distinct from both.

2.2 Comparison with the selection of strongly lensed galaxies in other wavebands

Herschel surveys have demonstrated that at $500 \mu\text{m}$ (600 GHz) strongly lensed galaxies with $S_{500\mu\text{m}} \geq 100 \text{ mJy}$, close to the detection limit of next generation space-borne CMB experiments with telescopes of the $\simeq 1.5 \text{ m}$ class operating at the diffraction limit, amount to $\simeq 25\%$ of the total counts [24, 38, cf. upper left panel of Fig. 3]. A similar fraction was found at the completeness limit ($\simeq 20 \text{ mJy}$) of the SPT survey at 220 GHz [5]. Such high fractions are a direct consequence of the extreme steepness of (sub-)mm counts of extragalactic sources due to the unique combination of steep cosmological evolution with a strongly

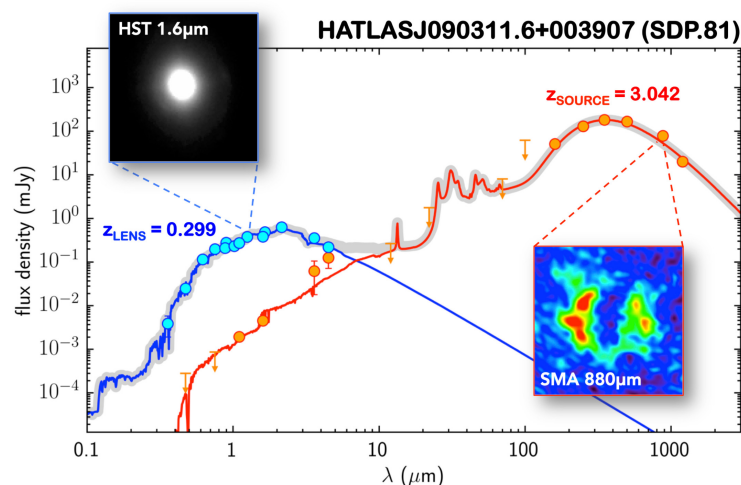


Figure 5. SEDs of the strongly lensed galaxy SDP 81 at 3.042 detected by the *Herschel* Astrophysical Terahertz Large Area Survey [H-ATLAS; 36] and imaged with the Sub-Millimeter Array (SMA) at 880 μm [15] and of the foreground lens at $z = 0.299$ imaged with the Wide Field Camera 3 (WFC3) on the Hubble Space Telescope [HST; 37]. As is generally the case, the lens is a spheroidal galaxy in passive evolution, hence very faint at sub-mm wavelengths; indeed it is essentially invisible in the SMA image. The lensed source is dust-enshrouded, hence bright in the sub-mm but very faint in the optical and essentially invisible in the WFC3/HST image.

negative K-correction³. They are an exclusive property of (sub-)mm surveys: searches in other wavebands have yielded fractions of $\simeq 0.1\%$ [41, 42, 43].

Not only the strongly-lensed fractions are high, but also the selection is easy done, with close to 100% efficiency [44, 15], while it remains a significant challenge in other wavebands [45]. The other extragalactic sources brighter than the detection limits of next generation CMB experiments are either $z \lesssim 0.1$ galaxies or radio sources (mainly blazars), that can be identified using existing all-sky optical or radio catalogs.

In the case of space-borne experiments, the selection can be done directly on survey data. As illustrated by the upper right-hand panel of Fig. 3, the redshift distribution of dusty galaxies detected by these experiments is highly bimodal. On one side we have nearby late-type galaxies, almost all at $z \leq 0.06$; on the other side we have dust enshrouded, hence optically very faint, gravitationally lensed galaxies at $z \geq 1$ and up to $z > 4$. This strong difference in redshift translates in a clear difference in sub-mm colours, high- z galaxies being much redder than the local ones; radio sources have still redder colours (see Fig. 4). This is specific to searches with these experiments. Selections in other wavebands need spectroscopy or other ancillary data. This is true also for ground-based surveys which provide photometry in the Rayleigh-Jeans region where colours are largely redshift-independent. On the other hand, the discrimination of strongly lensed galaxies will be greatly eased by the wealth of multi-wavelength data over the entire sky that will be available in the coming decade.

In addition to the much more efficient selection, other critical advantages of CMB experiments over other facilities that will generate large gravitational lens catalogues [e.g., *Euclid*, Gaia, SKA; 46] are:

³ The steep increase with increasing frequency of the dust emission spectrum at (sub-)mm wavelengths ($L_\nu \propto \nu^\alpha$ with $\alpha \simeq 3.5\text{--}4$) translates into a fast increase of the observed flux density with increasing redshift (negative K-correction). Such increase may compensate and even exceed the decrease due to increasing distance [39, 40]

- compared to optical/near-IR surveys, they detect earlier (higher redshift) phases of galaxy evolution, characterized by intense, dust-enshrouded star-formation activity;
- the photometry of detected galaxies will be only very weakly contaminated by the foreground lens, even in the case of close alignment along the line-of-sight (see Fig. 5); while the lensed galaxies are heavily dust enshrouded, hence bright at sub-mm wavelengths but faint in the optical, the foreground lenses are mostly massive early-type galaxies in passive evolution, hence optically bright but almost invisible in the sub-mm;
- the all-sky coverage maximizes the detections of the rare brightest sources, with the most extreme magnifications, optimally suited for follow-up, as demonstrated by *Planck*: the magnification factors of “*Planck*’s dusty GEMS” are estimated to be of up to 50 [30];
- the mm/sub-mm selection, with its strongly negative K-correction, allows us to extend the detection of sources and lenses to much higher redshifts than in any other waveband.

2.3 Astrophysics and cosmography with strong lensing

The extreme magnifications of dusty galaxies detected by CMB experiments makes them trivially easy targets for ALMA, NOEMA, SMA etc., and the foreground lenses will almost certainly be detectable by large optical telescopes and in, e.g., *Euclid* imaging. Follow-up observations will allow us to address major astrophysical issues [e.g., 43].

CMB experiments with arcmin resolution both from the ground and from space will drive a real breakthrough in the study of early evolutionary phases of galaxies, paving the way to answer major, still open problems like: which are the physical mechanisms shaping the galaxy properties [47, 48]: in situ processes? interactions? mergers? cold flows? How feedback processes work? To settle these issues we need direct information on the structure and the dynamics of high- z galaxies. But these are compact, with typical sizes of 1–2 kpc [e.g., 49, 50], corresponding to angular sizes of 0.1–0.2 arcsec at $z = 2$ –3. Thus they are hardly resolved even by ALMA and by the HST. If they are resolved, high enough signal-to-noise ratios per resolution element are achieved only for the brightest galaxies, not representative of the general population.

Strong gravitational lensing provides a solution. CMB surveys will detect the brightest (sub-)mm strongly lensed galaxies in the sky, with extreme magnifications, up to several tens [30]. Since lensing conserves surface brightness, the effective angular size is stretched by an average factor $\mu^{1/2}$, substantially increasing the resolving power. A spectacular example are ALMA 0.1 arcsec resolution observations of PLCK G244.8+54.9 at $z \simeq 3.0$ with $\mu \simeq 30$ [51] which reached the astounding spatial resolution of $\simeq 60$ pc, substantially smaller than the size of Galactic giant molecular clouds.

Cañameras et al. [51] also obtained CO spectroscopy with an uncertainty of 40–50 km/s. This spectral resolution makes possible a direct investigation of massive outflows driven by AGN feedback at high z , with predicted velocities of $\sim 1000 \text{ km s}^{-1}$ [52]. AGN driven outflows are a key ingredient of current galaxy evolution models since they provide the most plausible explanation for the deviation of the galaxy stellar mass function from the halo mass function at large masses, i.e. for the low star-formation efficiency in massive halos: only less than 10% of baryons initially present in such halos are used to form stars. However, until very recently, with few exceptions [53], high- z outflows were detected only in ionized gas [54]. Thus information on the effect of feedback on the direct fuel of star formation, molecular gas, has been largely missing during the epoch of the most active cosmic star formation.

Due to the weakness of spectral signatures of molecular outflows, observational progress has been difficult. Gravitational lensing allows us to overcome these difficulties. Spilker et al. [55] were able to detect, by means of ALMA spectroscopy, a fast (800 km/s) molecular outflow in a strongly lensed galaxy at $z = 5.3$, discovered by the SPT survey. The outflow carries mass at a rate close to the SFR, thus removing a large fraction of the gas available for star-formation. Cañameras et al. [56] detected a molecular wind signature in the strongly lensed galaxy PLCK G165.7+49.0, discovered by *Planck*, at $z = 2.236$, with magnification factors between 20 and 50 in most of the source. Strongly lensed galaxies detected by CMB experiments will be obvious targets for the next generation Very Large Array (ngVLA) that will provide accurate estimates of the molecular outflow masses and mass loss rates up to $z \simeq 4$ [57]. The proposed NASA flagship Origins Space Telescope [OST; 58, 59] would detect molecular, neutral, and warm ionized phases of outflows up to higher redshifts, although with a spatial resolution lower than ngVLA. AGN-driven outflows also produce a bubble of hot gas, potentially detectable via its Sunyaev-Zeldovich effect [SZE; 60, 61]. The first detection of the SZE from a hyperluminous quasar at $z = 1.71$, obtained by means of ALMA observations, was reported by Lacy et al. [62] who, from these measurements, derived constraints on the energetics of the wind.

The high redshifts of magnified galaxies imply high redshifts of foreground lenses. Optical follow-up allows us to investigate the total (visible and dark) mass of the lensing galaxies, their density profiles, dark matter sub-structures at higher redshifts than in the case of optical selection. For example, the spectroscopic redshift of the foreground deflector of the strongly lensed galaxy PLCK G244.8+54.9 ($z = 3.005$), measured by Cañameras et al. [63], was found to be exceptionally high, $z = 1.525$. This illustrates the power of the (sub-)mm selection of strongly lensed galaxies to push the study of dark matter and baryon assembly up to high redshifts.

The samples of thousands of strongly lensed galaxies provided by CMB experiments will also be a powerful tool to measure cosmological parameters [43, 64]. The lens equation contains ratios of angular diameter distances. Hence observables of lensed systems (redshifts of the source and of the lens, Einstein radius, velocity dispersion of the lens) can be used to estimate Ω_m , Ω_Λ and the parameters of the dark energy equation of state. These determinations will not be as precise as those obtained from CMB data, but will provide valuable independent tests of the cosmological model, will allow to look for unrecognized selection effects and to break degeneracies in the interpretation of CMB data. Also, the strong lensing optical depth depends on the abundance and redshift distributions of potential wells acting as deflectors, hence on density parameters, on the dark energy equation of state and its evolution and on the amplitude, σ_8 , of the primordial perturbation spectrum. Distortions of Einstein rings or giant arcs could offer a direct method to detect sub-halos, i.e. to constrain warm dark matter [65]. Lenses at high redshift are particularly valuable to determine the statistics of perturbations along the line of sight [43].

2.4 Local dusty galaxies

Herschel surveys have shown that the surface density of local dusty galaxies brighter than $S_{500\mu\text{m}} = 100$ mJy is $\simeq 1 \text{ deg}^{-2}$ and that their redshift distribution peaks at $z = 0.02\text{--}0.03$ [upper right panel of Fig. 3; 24]. A survey with a space borne $\simeq 1.5$ m telescope will detect tens of thousands of them. By the time when next generation CMB experiments will fly several wide-angle redshift and photometric surveys will be available, providing distance information for the majority, if not all of them [11]. Combining these data with available or forthcoming data in different wavebands (radio, IRAS, AKARI, WISE, Euclid, GALEX, ROSAT, eROSITA ...) it will be possible to determine, for each galaxy type and as a function of stellar mass, the distribution of dust temperatures and masses, the SFR function, the relationship between

star formation and nuclear activity, the contributions of newborn and evolved stars to dust heating, and more. The sample of local galaxies will also be large enough for clustering studies, i.e. to relate the properties of galaxies to the underlying dark matter field and to the properties of their dark matter haloes, as well as to investigate the link between galaxies of different types and their environments.

The surface density of local galaxies at the SPT completeness limit at 220 GHz (20 mJy) is of $\simeq 0.05 \text{ deg}^{-2}$ (lower left panel of Fig. 3), i.e. a factor of $\simeq 20$ lower than achieved by a space-borne 1.5 m telescope at 600 GHz. However, as shown by the SED of M 61 scaled down by a factor of 10 (Fig. 2), ground based surveys will detect, for the nearest low- z galaxies, also the radio emission powered by star formation. At mm wavelength such radio emission is expected to be dominated by free-free emission [66] which is an excellent measure of the instantaneous SFR since it scales with the ionizing luminosity and is unaffected by extinction. Its measurement will allow us to recalibrate the relation between dust emission (which may be contributed in part by dust heating from old stars) and SFR. According to the calculations by Mancuso et al. [67], the surface density of star-forming galaxies detected via their radio emission at 95 GHz by SPT-like experiments, i.e. brighter than $S_{95\text{GHz}} \simeq 10 \text{ mJy}$, is of $\simeq 12 \text{ sr}^{-1}$. We caution, however, that the measurement of the free-free emission requires the separation of the non-thermal (synchrotron) and dust contributions. This is very difficult to do accurately, especially because of uncertainties on the synchrotron spectrum [68].

Another open issue is the connection between nuclear radio activity and star formation. *Planck* has detected evidence of cold dust associated to a handful of nearby radio sources, based on their rising spectra at mm wavelengths [69]. The much deeper surveys carried out by next-generation experiments can push the investigation to much more distant objects.

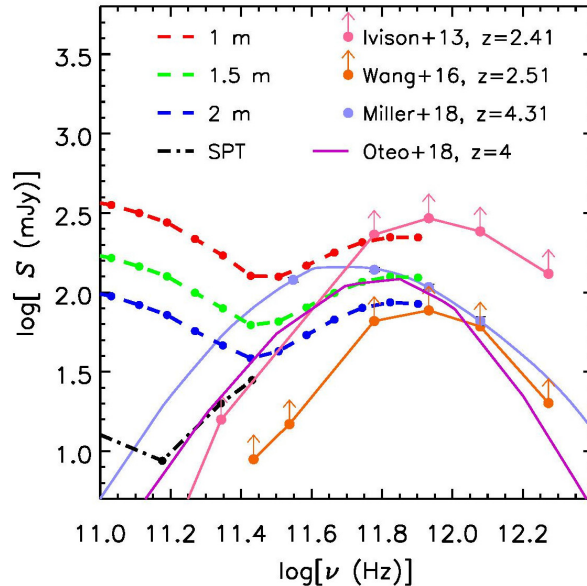


Figure 6. SEDs of spectroscopically confirmed sub-mm bright high- z proto-clusters detected by Ivison et al. [70], Wang et al. [71], Miller et al. [72] and Oteo et al. [73], compared with (from top to bottom) the detection limits of diffraction limited space-borne telescopes of 1, 1.5 and 2 m size, and with the SPT completeness limit. The flux densities by Ivison et al. [70] and Wang et al. [71] are shown as lower limits because they include the contributions of member galaxies across a $\sim 100 \text{ kpc}$ region, substantially smaller than the expected proto-cluster size ($\sim 500 \text{ kpc}$).

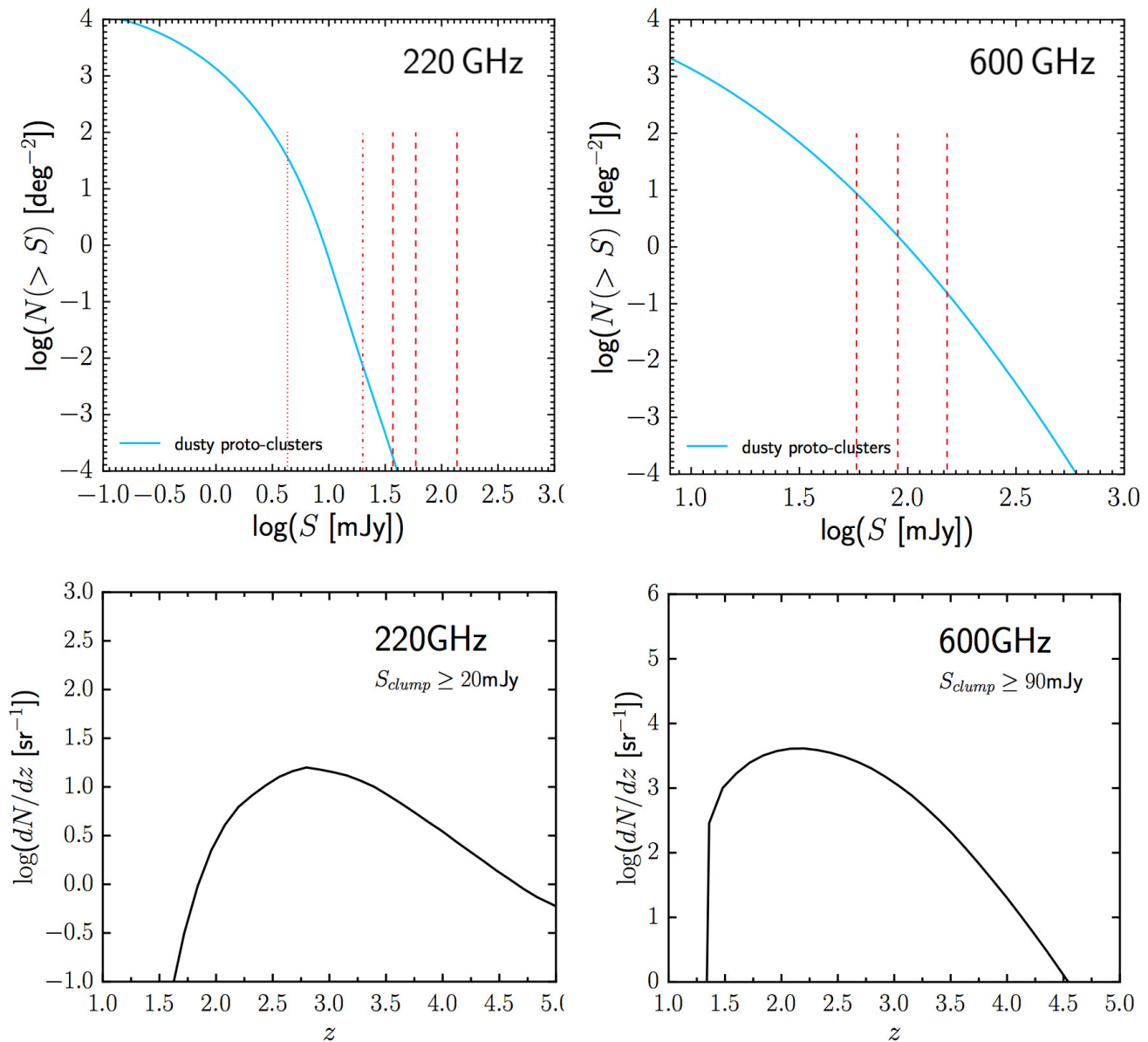


Figure 7. Integral counts and redshift distributions of proto-clusters at 220 GHz and 600 GHz (1.4 mm and 500 μm , respectively) predicted by Negrello et al. [74]. The vertical lines in the upper left panel show, from left to right, the 5σ confusion limit for a 6 m telescope, the SPT completeness limit and the 5σ detection limits for 2, 1.5 and 1 m telescopes operating at the diffraction limit. Only the three latter limits, at 600 GHz, are shown in the upper right-hand panel. The lower panels show the redshift distributions at the SPT completeness limit at 220 GHz (20 mJy, left) and at the 5σ detection limit (90 mJy) for a 1.5 m telescope at 600 GHz (right).

3 EARLY PHASES OF CLUSTER EVOLUTION

Understanding the full evolutionary history of present-day galaxy clusters is of fundamental importance for the observational validation of the formation history of the most massive dark matter halos, a crucial test of models for structure formation, and for investigating the impact of environment on the formation and evolution of galaxies. Because of their deep potential wells, clusters may preserve fingerprints of the

physical processes responsible for triggering and suppression of star formation and black hole activity. Also, clusters of galaxies have historically been powerful probes of cosmological parameters [e.g., ref. 75].

This has driven extensive searches for high redshift galaxy proto-clusters in the past two decades [for a review see ref. 76]. Classical systematic cluster searches were carried out via X-ray [e.g., refs. 77, 78], Sunyaev-Zeldovich [SZ; 79, 80, 81, 82] and optical/near-infrared [83, 84, 85, 86] surveys. These surveys, however, have yielded only a handful of confirmed proto-cluster detections at $z \gtrsim 1.5$ [76]. The reason is that, while at $z \lesssim 1-1.5$ cluster cores are dominated by passive early-type galaxies and are filled by hot gas, at higher z cluster members enter the dust-obscured star-formation phase and the intergalactic gas is no longer necessarily at the virial temperature. In fact, several programs have found an inversion of the star formation–density relation at $z \gtrsim 1.3$. At lower redshifts, it has long been known that there is a well defined increase of the passive elliptical and lenticular (denoted S0) population with increasing density [87]. Dense cluster cores are preferentially populated by massive, passively evolving, early-type galaxies. Star-forming galaxies are generally found in the cluster outskirts and in the field⁴. At higher redshifts, however, cluster cores are found to have an increasing population of strongly star-forming, luminous infrared galaxies [88, 89, 90]. Their specific SFR increases rapidly from $z \sim 0.2$ to $z \sim 1.3$, mostly driven by the activation of star formation in early-type galaxies. The star-formation activity in cluster core ($r < 0.5$ Mpc) galaxies reaches the field level at $z \gtrsim 1.2$.

So far, most of the detections of high- z (proto-)clusters have been obtained either as by-products of large spectroscopic or multi-band photometric surveys, or using biased tracer techniques [76]. The latter techniques consists in targeting the immediate environment of tracers of massive forming systems, like high redshift radio galaxies and QSOs, Ly α blobs and bright sub-millimeter galaxies. The data sets collected in these ways are obviously highly heterogeneous, affected by strong, hard to quantify selection biases and only sparsely sample the redshift distribution of (proto-)clusters. They are therefore unsuitable to obtain a complete picture of the build-up of galaxy clusters over cosmic time.

The very fact that member galaxies are increasingly infrared luminous with increasing redshift, means that (sub-)mm surveys are the most effective tool to detect high- z proto-clusters. They are rare objects and therefore the multi-steradian CMB surveys are optimal to find at least the (sub-)mm brightest ones. A blind search on *Planck* maps was carried out by Planck Collaboration Int. XXXIX [91] at 5' resolution. They looked for intensity peaks with “cold” sub-mm colours, i.e. with continuum spectra peaking between 353 and 857 GHz, consistent with redshifts $z > 2$ for typical dust emission spectra. *Herschel*/SPIRE follow-up of 234 *Planck* targets with such colours showed that almost all of them correspond to strong over-densities of red 350 and 500 μ m sources in comparison to reference SPIRE fields [92]. Further investigations of *Planck* proto-cluster candidates were carried out by refs. [93, 94, 95].

However, the *Planck*'s angular resolution of $\simeq 5'$, corresponding to a physical size of about 2.5 Mpc at $z = 1.5-2$, is not optimal for detecting proto-clusters. By means of detailed simulations based on a physically motivated galaxy evolution model, Negrello et al. [74] showed that essentially all *Planck*'s cold peaks can be interpreted as positive Poisson fluctuations of the number of high- z proto-clusters of dusty galaxies within the *Planck* beam, rather than being individual clumps of physically bound galaxies.

The study [88] of 274 clusters with $0.3 \leq z \leq 1.5$ from the *Spitzer* InfraRed Array Camera (IRAC) Shallow Cluster Survey, using *Herschel*/SPIRE 250- μ m imaging, showed that the density of IR-emitting cluster members clearly exceeds that of the background field level only within 0.5 Mpc of the cluster centre. A linear scale of 0.5 Mpc corresponds to an angular scale of about 1' at redshifts in the range

⁴ Field galaxies are those that do not reside in overdense regions.

1.5–2.5, close to the PICO/CORE/CMB Bharat FWHM at 800 GHz and to the resolution of CMB-S4 and of the Simons Observatory at mm wavelengths. Thus, next generation CMB experiments will be optimally suited to detect the bright cluster cores of the kind discovered by Ivison et al. [70] at $z = 2.41$, Wang et al. [71] at $z = 2.51$, Miller et al. [72] at $z = 4.31$ and Oteo et al. [73] at $z = 4.0$ (see Fig. 6). Spectroscopic confirmations of additional proto-clusters detected at sub-mm wavelengths have been most recently reported by Gómez-Guijarro et al. [96] and Lacaille et al. [97]. Figure 6 shows that proto-clusters bright enough to be detected by next generation CMB experiments exist out to $z \gtrsim 4$. Note that, as argued by De Zotti et al. [11], proto-clusters stand out as intensity peaks in background-subtracted maps more clearly than in surveys of point sources. This is because such intensity peaks include the contribution of all member galaxies, including those below the point source detection limit, that may dominate the integrated flux density.

How many dusty proto-cluster detections can we expect? The predictions of the model by Negrello et al. [74], that reproduced all the relevant data, are shown in Fig. 7. Space-borne experiments like PICO/CORE/CMB Bharat will detect many tens of thousands of these objects, with a predicted redshift distribution peaking at $z \simeq 2$ and extending out to $z \simeq 4.5$. Ground based instruments will preferentially detect proto-clusters at higher redshifts, out to $z \gtrsim 5$, with a distribution having a broad peak around $z \simeq 2.75$. Since high- z clusters are expected to be rare, the number of detections will be of only $\simeq 10^{-2} \text{ deg}^{-2}$ at the SPT completeness limit at 1.4 mm. The number of detections rapidly increase with decreasing detection limit, reaching $\simeq 40 \text{ deg}^{-2}$ at the SPT confusion limit. This will constitute a real breakthrough in the observational determination of the formation history of the cluster-sized dark matter halos. Follow-up observations will characterize the properties of member galaxies, probing the galaxy evolution in dense environments and shedding light on the complex physical processes driving it.

CMB experiments will also allow us to investigate the evolution of galaxy populations in clusters detected by other means, e.g. via their X-ray emission or via the thermal SZ effect. De Zotti et al. [11, their Fig. 4] showed that space-borne CMB experiments with telescopes of the 1.5 m class will detect, at 800 GHz the dust emission of the brightest $M \simeq 10^{14} M_{\odot}$ clusters and of typical $M \simeq 10^{14.5} M_{\odot}$ clusters at $1 \lesssim z \lesssim 1.5$. More massive clusters will be detected over broader redshift ranges. Figure 8 shows that SPT-like ground based surveys observing at 220 GHz will perform similarly or only slightly worse. For comparison, *Herschel* has allowed the study of the IR emission from clusters up to $z \simeq 1.7$ [89], but the sample comprises only 11 clusters. The *Herschel* data have shown large variations in cluster properties, highlighting the need for evolutionary studies of large, uniform cluster samples over a broad redshift range. Next generation CMB experiments will fulfill this need. Stacking will allow us to carry out a statistical investigation of the evolution of the cluster IR emission to fainter levels. Targets for stacking will abound. eROSITA (extended ROentgen Survey with an Imaging Telescope Array) will provide an all-sky deep X-ray survey detecting $\sim 10^5$ galaxy clusters out to $z > 1$ [98]. CMB experiments themselves will detect tens of thousands of clusters via the SZ effect [2, 99, 21, 22].

This will be important to investigate the evolution of the specific SFR in dense environments. In addition, the dust emission in galaxy clusters will impact the completeness of SZ surveys and will distort the SZ signal [100], affecting the cosmological results derived from SZ observations. While the latter effect was shown to be negligible in *Planck*'s case [100], it will be important for the much deeper next generation surveys.

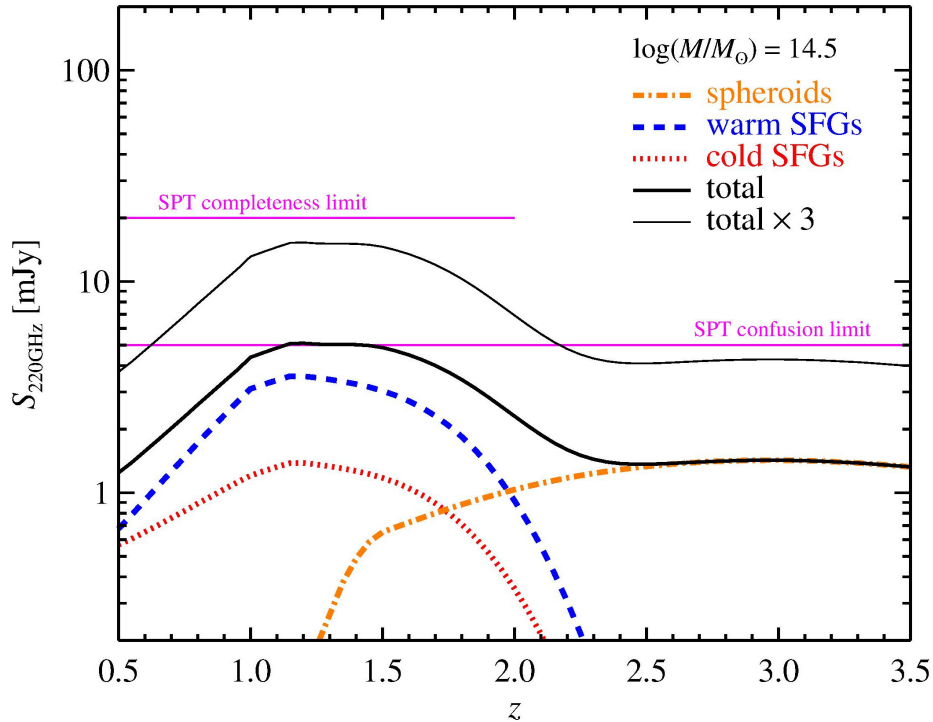


Figure 8. Expected flux density at 220 GHz due to the integrated dust emission from member galaxies of a cluster with $M = 10^{14.5} M_{\odot}$ as a function of the cluster redshift (solid thick black curve). The cluster luminosity includes contributions from normal late-type and starburst galaxies (warm and cold SFGs, respectively) and from proto-spheroidal galaxies (spheroids), computed using the model by Cai et al. [25]. The thinner upper black curve is a factor of 3 higher and illustrates the large variance of the cluster IR emission at fixed mass [88, 89]. It must be noted that the *Planck* and the SPT surveys have detected $z > 0.5$ clusters with masses of more than $10^{15} M_{\odot}$. The upper horizontal line corresponds to the SPT completeness limit, the lower one to its 5σ confusion limit.

4 RADIO SOURCES

4.1 Blazar physics

Although substantial progress on the characterization of mm and sub-mm properties of extragalactic radio sources has been made in recent years mainly thanks to surveys with WMAP, *Planck*, the SPT and the ACT, the available information is still limited. The overwhelming majority of extragalactic radio sources detectable in the frequency range of CMB experiments are blazars, i.e. sources whose radio emission is dominated by relativistic jets collimated by intense magnetic fields and closely aligned with the line of sight. These objects with extreme properties are of special interest since they are also strong gamma-ray sources: about 90% of the firmly identified extragalactic gamma-ray sources are blazars.

Accurate source counts over large flux density intervals provide key constraints on evolutionary models of these sources. Just because high frequency surveys are still far less extensive than those at low radio frequencies, evolutionary models for blazar populations, Flat Spectrum Radio Quasars (FSRQs) and BL Lacertae sources (BL Lacs), are far less advanced than those for steep-spectrum radio sources. For example, while clear evidence for downsizing⁵ was reported in the case of steep-spectrum sources [103, 104], the

⁵ “Downsizing” refers to the very different evolutionary behaviour of high- and low-luminosity sources, in the sense that the redshift of the peak space density of sources decreases with luminosity.

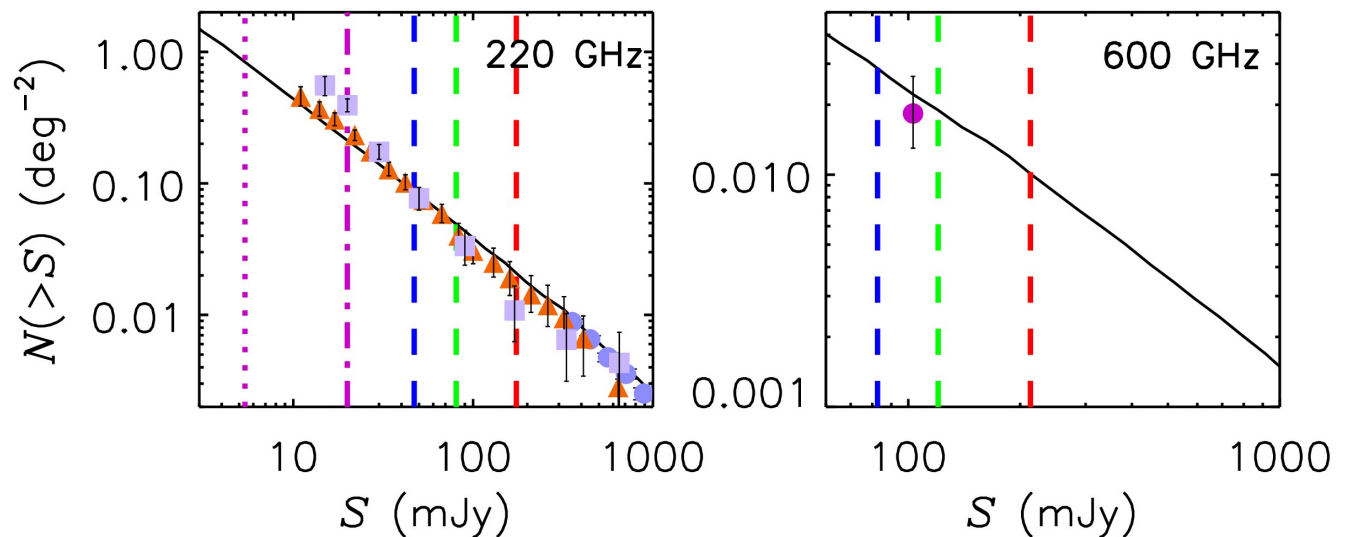


Figure 9. Integral number counts of radio sources at 220 and 600 GHz. The vertical dashed lines show the 5σ confusion limits for a space-borne experiment with a 1 m, 1.5 m and a 2 m telescope (from right to left) operating at the diffraction limit. The dot-dashed and dotted vertical lines on the left panel show the completeness limit of the SPT survey and the 5σ confusion limit for the SPT telescope, respectively. The data points on the left panel are from Mocanu et al. [5, SPT, orange triangles], Marsden et al. [20, ACT, lavender squares], Planck Collaboration. XIII. [101, light blue circles]; the data point on the right panel is from Bonato et al. [102] and is based on *Herschel* survey data. The solid black lines are predictions of the Tucci et al. [27] model.

available data are insufficient to test if this is the case also for FSRQs; for BL Lacs the constraints on evolutionary parameters are even weaker. This situation hampers sharp tests of unified models.

Planck has already provided strong indications of the crucial role of blazar photometry up to sub-mm wavelengths to get information on the energy spectrum of relativistic electrons responsible for the synchrotron emission, with interesting implications for the acceleration mechanisms [69].

Another interesting open question is the geometry of the emitting regions. The most commonly used model for the spectral energy distribution (SED) of compact, radio loud Active Galactic Nuclei (AGNs) is a leptonic, one-zone model, where the emission originates in a single component. The SEDs typically consist of two broad-band bumps; the one at lower frequencies is attributed to synchrotron radiation while the second, peaking at gamma-ray energies, is attributed to inverse Compton. The one-zone model is generally found to provide an adequate approximation primarily because of the limited observational characterization of the synchrotron SED, with fragmentary data over a limited frequency range. However VLBI images show multiple knots often called “components” of the jet. The standard model [105] interprets the knots as due to shocks that enhance the local synchrotron emission.

The spectrum is explained as the result of the superposition of different synchrotron self-absorbed components in a conical geometry. The synchrotron self-absorption optical depth scales as $\tau_{\text{sync}} \propto B_{\perp}^{(p+2)/2} \nu^{-(p+4)/2}$ where B_{\perp} is the magnetic field component perpendicular to the electron velocity and p is spectral index of the energy distribution of relativistic electrons (typically, $p \simeq 2.5$). Thus τ_{sync} increases towards the nucleus as the magnetic field intensity and its ordering increases, but is strongly frequency dependent: the emission at higher and higher frequencies comes from smaller and smaller distances from the central engine.

Thus the mm and sub-mm emissions provide information on the innermost regions of the jets, where it is optically thin, while the emission at longer wavelengths is affected by self-absorption. Interestingly millimeter-wave flux densities of FSRQs turn out to be strongly correlated with simultaneous gamma-ray fluxes [106, 107]. The strongest gamma-ray flares were found to occur during the rising/peaking stages of millimeter flares. This suggests that the gamma-ray flares originate in the millimeter-wave emitting regions of these sources.

The available data are mostly at cm (or longer) wavelengths and are scanty at (sub-)mm wavelengths because of the limited sky areas covered by the available surveys. Ground-based experiments with ~ 6 m telescopes, like CMB-S4 and the Simons Observatory, will detect thousands of blazars per sr at millimeter wavelengths (Fig. 9). Extrapolating the 8.4 GHz flux densities of the 18 $z > 4$ FSRQs listed by Caccianiga et al. [108] using the measured 1.4–8.4 GHz spectral indices we find that a large fraction of them will be detected by these experiments, including the highest redshift blazar known, GB6J090631 + 693027 at $z = 5.47$. The radio selection, being unaffected by obscuration, provides an unbiased census at least of the radio-loud fraction of high- z AGNs.

The most luminous high- z FSRQs were found to have black holes with the largest masses, up to $\simeq 4 \times 10^{10} M_{\odot}$ [S5 0014 + 813 at $z = 3.366$; 109]. Such objects have particularly hard mm-wave spectra, are rare and bright because of the Doppler boosting of their flux densities. CMB surveys are thus optimally suited to detect them. Since the flux boosting occurs for jets closely aligned with the line of sight ($\theta < 1/\Gamma$, $\Gamma \sim 15$ being the bulk Lorentz factor), for each FSRQ there are other $2\Gamma^2$ (i.e. hundreds) sources of similar intrinsic properties but pointing elsewhere. This means that blazars are very efficient probes of extreme super-massive black holes at high z .

Very large black hole masses at high z are puzzling because it is challenging to grow a stellar mass seed black hole to $> 10^9 M_{\odot}$ in the limited age of the universe. It is even more challenging in the case of jetted quasars because it is commonly believed that the jets are associated with rapidly spinning black holes. But then the radiative efficiency is large and the mass growth is slower. Yet at least 4 FSRQs have been discovered at $z > 5$; one of them (SDSS J013127.34–032100.1 at $z = 5.18$) has estimated black hole mass of $\simeq 1 \times 10^{10} M_{\odot}$ [110].

Next-generation space-borne CMB experiments with $\simeq 1.5$ m telescopes, like PICO, will provide, for the first time, samples of hundreds of blazars blindly selected at sub-mm wavelengths. An important property of surveys from space is that they provide simultaneous photometry over a broad frequency range, thus overcoming the complications due to variability and allowing us to directly connect the observed SED to the physical processes operating along the jet.

4.2 Earliest and latest phases of radio activity

Large-area surveys at frequencies of tens to hundreds GHz will also detect the rare but very interesting sources associated to the earliest and to the latest stages of the radio-AGN evolution, both characterized by emissions peaking in this frequency range [111]. It is now widely agreed that extreme gigahertz peaked spectrum (GPS) sources correspond to the early stages of the evolution of powerful radio sources, when the radio emitting region grows and expands within the interstellar medium of the host galaxy, before plunging in the inter-galactic medium and becoming an extended radio source. There is a clear anti-correlation between the peak (turnover) frequency and the projected linear size of GPS sources, suggesting a decrease of the peak frequency as the emitting blob expands. The identification of these sources is therefore a key element in the study of the early evolution of radio AGNs. High-frequency surveys will detect these sources very close to the moment when they turn on.

Possible examples of extremely young sources are the six narrow-line Seyfert 1 galaxies detected by Lähteenmäki et al. [112] at 37 GHz with flux densities of 270–970 mJy but undetected by the FIRST survey, complete down to $\simeq 1$ mJy at 1.4 GHz, carried out about 20 yr ago. One possibility is that the new observations have discovered newly triggered radio activity from nuclei that were essentially radio silent two decades ago.

Young radio activity was recently discovered by Bruni et al. [113] in the nuclei of 8 out of 13 ($\simeq 61\%$) hard X-ray selected giant radio galaxies for which they had enough spectral coverage to ascertain the presence of a peak. Two of the 8 sources have a peak frequency > 10 GHz and at least one is bright enough to be clearly detected by next generation CMB experiments.

The multi-frequency surveys by next generation CMB experiments will provide an unbiased view of the frequency of these phenomena and will measure their high frequency SEDs, shedding light on their nature. These data will enable studies of the launching of relativistic jets as well as of the evolutionary paths that young AGNs take on their way to becoming fully-evolved, powerful radio sources.

Large area (sub-)mm surveys will also allow us to investigate the late stages of the AGN evolution in elliptical galaxies, characterized by low radiation/accretion efficiency. These manifest themselves via a nuclear radio emission described by advection-dominated accretion flows (ADAFs) and/or by adiabatic inflow-outflow solutions (ADIOS). Doi et al. [114] have found that at least half of their sample of 20 low-luminosity AGNs with compact radio cores show radio spectra rising at least up to 96 GHz, consistent with the ‘sub-millimetre bump’ predicted by an ADAF model. Again CMB surveys will determine the abundance of these objects and their SED measurements will clarify the origin of the emission.

Predictions of the expected number of detections of early and late phases of radio activity are limited to ≤ 30 GHz [111, 115]. They suggest that at 20–30 GHz hundreds of these objects can be detected by ground-based experiments. Space-borne experiments are confusion-limited to much brighter flux densities, implying a detection rate at least one order of magnitude lower. The number of detections is predicted to drop rapidly with increasing frequency [116, 117].

4.3 The extragalactic transient sky

High-sensitivity and high-angular-resolution CMB surveys also offer a unique opportunity to carry out an unbiased investigation of the largely unexplored extragalactic mm/sub-mm transient sky [118]. So far measurements have been limited to follow-up of objects detected at other wavelengths, with limited success partly because of the need for excellent weather conditions or because the events were too short-lived to detect without very rapid reaction times. CMB surveys will allow us to discover new, unknown transient sources in this band.

One example of transient phenomena are outbursts from AGNs and especially from blazars. Outbursts and, more generally, variability, provide key information on the flow of the plasma within the relativistic jets. Signatures of evolving shocks in the strongest radio flares were seen by Planck Collaboration. XLV. [69] although high frequency light curves are generally quite similar (approximately achromatic variability). These results are compatible with the standard shocked jet model, but other interpretations are possible. Definite conclusions are currently hampered by the limited statistics. This limit will be overcome by next generation CMB experiments from space which will provide multi-epoch simultaneous observations of large blazar samples over a broad frequency range. This will allow us to study their variability properties as a function of flux density and spectral shape.

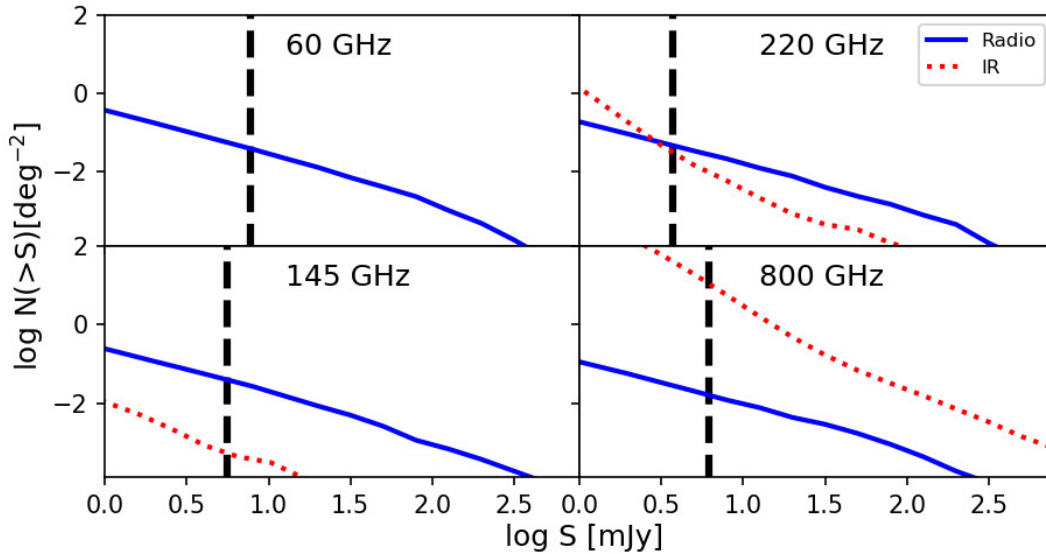


Figure 10. Estimated integral number counts in polarized intensity of radio sources and of dusty galaxies (IR) at 60, 145, 220 and 800 GHz. The contribution of dusty galaxies is completely negligible at 60 GHz. The vertical dashed black lines show the 5σ detection limits for a space-borne instrument with a 1.5 m telescope and state-of-the-art sensitivity derived from simulations similar to those described in De Zotti et al. [11]. The present simulations assumed log-normal distributions of the polarization fractions with mean and dispersion of 2.14% and of 0.9%, respectively, for radio sources and of 1.4 and 1%, respectively, for dusty galaxies.

Perhaps even more interesting is the possibility of detecting radio afterglows of gamma-ray bursts (GRBs). Afterglows often have a spectral peak in or near the mm range [117], with emission lasting over days to weeks. One candidate object with properties broadly consistent with a GRB afterglow was tentatively detected by Whitehorn et al. [119] on SPT data over 100 deg^2 with an observing time of 6,000 h, but the statistical significance of the detection was too low to completely rule out a fluctuation. GRB emission is expected to be less tightly beamed at these wavelengths than in gamma-rays. Thus afterglows not accompanied by detectable gamma-ray emission are expected to exist, but have not been detected yet. Blind surveys of large sky areas by next generation ground-based CMB experiments down to $\simeq 10 \text{ mJy}$ sensitivity can reveal these orphan afterglows and new, unknown sources. Multiple detections per year are expected. Even a non-detection will place interesting constraints on the shock dynamics and on the energy budget of the unknown GRB progenitors.

One example of unexpected phenomena that may show up at (sub-)mm wavelengths is the extraordinary extragalactic transient AT2018cow, with an estimated peak flux density of 94 mJy at $\simeq 100 \text{ GHz}$ [120]. This object may herald a new class of energetic transients which at early times are most readily observed at (sub-)mm wavelengths.

5 DETECTING SOURCES IN POLARIZATION

Accurate simulations [121] showed that, for a tensor-to-scalar ratio $r \simeq 10^{-3}$ (i.e. at levels predicted by models currently of special interest, such as Starobinsky's R^2 and Higgs inflation), the overall uncertainty on r is dominated by foreground residuals and that unresolved polarized point sources can be the dominant foreground contamination over a broad range of angular scales ($\ell \gtrsim 50$). A thorough understanding of the polarization properties of extragalactic sources is therefore crucial.

While the point source power spectra in total intensity are quite well constrained, estimates in polarization are obtained by coupling the counts in total intensity with distributions of the polarization fractions derived from lower frequency surveys. This implicitly assumes that such distributions are frequency-independent. Although this assumption is consistent with the available data [122, 123], there are substantial uncertainties and indeed variations are expected since emissions at different frequencies of flat-spectrum sources, that dominate in the relevant frequency range, come from different regions where the magnetic field properties are expected to be different.

Polarization measurements at $\gtrsim 100$ GHz are still scanty. Only a few tens of sources (all radio) were detected by *Planck* in the ‘extragalactic zone’ [11]. Galluzzi et al. [124] carried out ALMA high sensitivity polarimetric observations at 97.5 GHz of a complete sample of 32 compact extragalactic radio sources brighter than 200 mJy at 20 GHz; a detection rate of 97% was achieved.

Datta et al. [125] reported the detection of linear polarization at 148 GHz of 26 extragalactic sources with total flux density $S_{148\text{ GHz}} > 215$ mJy, 14 of which at greater than 3σ significance, during the first two seasons of the ACT polarization (ACTPol) survey, covering 680 deg^2 of the sky. Their results are consistent with a mean fractional polarization $\langle\Pi\rangle = 0.028 \pm 0.005$ and a standard deviation $\sigma_p = 0.054$, independent of total intensity.

Gupta et al. [126] investigated the polarisation properties of extragalactic sources in the SPTpol 500 deg^2 survey at 95 and 150 GHz down to 6 mJy. They found no evidence that the polarisation fraction depends on flux density. Assuming $\langle\Pi\rangle$ to be constant across flux bins they obtained, for radio sources, flux weighted $\langle\Pi^2\rangle = (8.9 \pm 1.1) \times 10^{-4}$ at 95 GHz and $\langle\Pi^2\rangle = (6.9 \pm 1.1) \times 10^{-4}$ at 150 GHz.

These results are consistent with the conclusion by Bonavera et al. [127] who applied stacking techniques to radio sources detected by *Planck* in total intensity, finding an average fractional polarization of $\simeq 3\%$, essentially independent of frequency from 30 to 353 GHz. A similar conclusion was reached by the independent analysis of Trombetti et al. [128].

The (sub-)mm polarization properties of dusty galaxies are essentially unknown. The only published measurement of the polarization degree averaged over the whole galaxy [129] yielded $\Pi \simeq 0.4\%$ at $850\text{ }\mu\text{m}$ for the prototype starburst galaxy M 82. A 99% confidence upper limit of 1.54% at the same wavelength was reported by Seiffert et al. [130] for the ultraluminous infrared galaxy (ULIRG) Arp 220. From the *Planck* dust polarization maps of the Milky Way, De Zotti et al. [11] found an average value of the Stokes Q parameter of about 2.7%. If this is typical of disk galaxies, their mean polarization degree averaged over all possible inclination angles is $\simeq 1.4\%$.

By applying the stacking techniques to a large sample of dusty galaxies drawn from the PCCS2 857 GHz catalogue, Bonavera et al. [131] estimated a median Π of $(2.0 \pm 0.8\%)$ at 353 GHz, consistent with the 90% confidence upper limit of 2.2% derived by Trombetti et al. [128]. The sample by Gupta et al. [126] includes 55 sources classified as dusty galaxies. No polarization signal was detected for these sources. The resulting 95% confidence level upper limits are $\langle\Pi^2\rangle < 16.9 \times 10^{-3}$ at 95 GHz and $\langle\Pi^2\rangle < 2.6 \times 10^{-3}$ at 150 GHz, consistent with earlier results.

These low values of Π are understood as due to the complex structure of galactic magnetic fields, with reversals along the line of sight, and to the disordered alignment of dust grains; both effects work to decrease the global polarization degree. Nevertheless, the current limits on the distribution of polarization fractions of dusty galaxies permit a contamination of CMB polarization maps comparable to that of radio sources down to 100–140 GHz, and dominant at higher frequencies [131, 128]. The amplitude of the power

spectrum of polarized dusty galaxies may be close to the level of CMB lensing B -modes and of primordial B -modes for $r \simeq 0.01$.

At variance with total intensity, in the case of polarization the detection limit is dictated by sensitivity, not by confusion noise. Hence, the spectacular improvement in sensitivity of next generation CMB experiments, compared to *Planck*, will allow a real breakthrough in the characterization of the polarization properties of extragalactic sources. Figure 10 shows the integral number counts in polarized intensity of radio sources and of dusty galaxies at 60, 145, 220 and 800 GHz obtained from the simulations described in De Zotti et al. [11]. The vertical dashed black lines show the 5σ detection limits for a space-borne instrument with a 1.5 m telescope and state-of-the-art sensitivity, derived from simulations made as described in De Zotti et al. [11], assuming log-normal distributions of the polarization fractions. For radio sources we adopted the same mean and dispersion (2.14% and of 0.9%, respectively) used by De Zotti et al. [11]. For dusty galaxies we adopted the value for our own Galaxy, averaged over inclinations (1.4%), with a dispersion of 1%. The estimated 5σ detection limits are 3.7 mJy at 220 GHz and 6.2 mJy at 800 GHz. At these limits the expected integral counts at 220 GHz are of $\simeq 160 \text{ sr}^{-1}$ radio sources and of $\simeq 100 \text{ sr}^{-1}$ dusty galaxies; at 800 GHz they are of $\simeq 50 \text{ sr}^{-1}$ radio sources and of $\simeq 36,000 \text{ sr}^{-1}$ dusty galaxies.

Under these assumptions, radio sources are the dominant population below $\simeq 200$ GHz. A comparison with the results reported by De Zotti et al. [11] who used a mean polarization fraction of 0.5% for dusty galaxies shows that the predicted counts are highly sensitive to the choice for this, highly uncertain, quantity.

As illustrated by Fig. 10, next generation CMB experiments will be capable of providing, for the first time, direct counts in polarization both for radio sources and for dusty galaxies, thus overcoming the current large uncertainties on the source power spectra in polarization. On one side this will allow a much better control of the extragalactic source contamination of CMB maps. This is particularly important in the 60–120 GHz frequency range, where diffuse polarized foreground emissions display a broad minimum.

On the other side, polarization observations enable us to understand geometrical structure and intensity of magnetic fields, particle densities and structures of emission regions. In the case of extragalactic radio sources, emission at mm/sub-mm wavelengths is synchrotron radiation arising close to the origin of the jet, on sub-parsec scales, generally unresolved even by the highest frequency very long baseline interferometry (VLBI) maps [132]. At these wavelengths the emission is expected to be optically thin, so that self-absorption and Faraday rotation are negligible. Then, in principle, the linear polarization degree can be as high as 60–80% if the magnetic field is ordered [133]. Hence, measurements of the polarization degree constrain the magnetic field geometry.

6 CONCLUSIONS

Thanks to their high sensitivity and to the coverage of large fractions of the sky, next generation CMB experiments will provide ground-breaking results in the field of extragalactic astrophysics. They will provide samples of several thousands of the brightest high- z strongly lensed, dusty galaxies, with extreme amplifications, up to $\mu \simeq 50$, and out to $z \gtrsim 6$. This will constitute an ideal data-base for high-resolution follow-up observations addressing the internal structure and kinematics of primordial galaxies, i.e. to understand the physical processes that drive the galaxy formation and early evolution across a broad redshift range, up to the re-ionization epoch.

CMB experiments will also provide unbiased, flux limited samples of tens of thousands of dense proto-cluster cores out to $z \gtrsim 4$, well beyond the reach of classical (optical, X-ray, SZ) cluster surveys that are

mostly limited to $z \lesssim 1.5$. They will effectively open a new window on the study of early phases of cluster formation, when their member galaxies were actively star forming and before the hot intergalactic medium was in place. This is crucial to observationally assess the formation history of the most massive dark matter halos, traced by clusters, a critical test of models for structure formation.

These experiments will also allow us to investigate, via direct detections complemented with stacking analyses, the evolution of the star-formation rate in virialized galaxy clusters detected by X-ray and SZ surveys (including those carried out by the experiments themselves), shedding light on the role of dense environments on galaxy evolution.

The data on radio sources will greatly improve our understanding of the evolutionary properties of FSRQs and BL Lac objects. They will also probe the jet physics in its innermost regions as well as the earliest and latest phases of radio activity. Particularly interesting is the possibility of getting an unbiased view of the abundance of candidate newly-born radio sources. These surveys also offer a unique opportunity to carry out an unbiased investigation of the largely unexplored mm/sub-mm transient sky, including the detection of predicted, but still unseen, “orphan” radio afterglows of GRBs as well as unexpected transient phenomena.

Furthermore, these experiments will provide the first, extensive, blind high-frequency census of the polarization properties of radio sources and of star-forming galaxies. This is essential to clean CMB maps at the level required to measure the faint primordial B -mode power spectrum. At the same time, mm/sub-mm polarization data on radio sources provide unique information on the geometry of the magnetic field on sub-pc scales, unresolved even by high-frequency VLBI observations. Polarimetry of dusty galaxies is informative on the structure of galactic magnetic fields.

CONFLICT OF INTEREST STATEMENT

The authors declare that the research was conducted in the absence of any commercial or financial relationships that could be construed as a potential conflict of interest.

AUTHOR CONTRIBUTIONS

GDZ has coordinated the work and written most of the text. MB, MN and ZYC have made model calculations and prepared Figs. 2, 3, 5, 6, 7, 8 and 9. TT and CB worked on the selection of strongly lensed galaxies detected by *Planck* and made Fig. 4. DH and MLC made the simulations and the source extraction on degraded SPT maps and produced Fig. 1. ZYC computed the redshift distribution of strongly lensed galaxies at 1.4 mm and the integrated flux density of cluster galaxies at 220 GHz as a function of redshift, and made a panel of Fig. 3 and Fig. 8. LL and JGN performed the simulations used to determine the detection limits in polarization and made Fig. 10. All authors critically reviewed the entire paper.

FUNDING

GDZ, CB and TT acknowledge financial support from ASI/INAF agreement n. 2014-024-R.1 for the *Planck* LFI Activity of Phase E2 and from the ASI/Physics Department of the university of Roma–Tor Vergata agreement n. 2016-24-H.0 for study activities of the Italian cosmology community. MB acknowledges support from the Italian Ministero dell’Istruzione, Università e Ricerca through the grant ‘Progetti Premiali 2012-iALMA’ (CUP C52I13000140001) and, together with CB and TT, from INAF under PRIN SKA/CTA FORECaST. DH acknowledges partial financial support from the Spanish Ministerio de Economía y

Competitividad (MINECO) project AYA2015- 64508-P and from the RADIOFOREGROUNDS project, funded by the European Commission's H2020 Research Infrastructures under the Grant Agreement 687312.

ACKNOWLEDGMENTS

We are grateful to the referees for a careful reading of the manuscript and many useful comments. GDZ acknowledges enlightening discussions on CMB experiments with S. Hanany and J. Delabrouille.

REFERENCES

- [1] Delabrouille J, de Bernardis P, Bouchet FR, Achúcarro A, Ade PAR, Allison R, et al. Exploring cosmic origins with CORE: Survey requirements and mission design. *JCAP* **4** (2018) 014. doi:10.1088/1475-7516/2018/04/014.
- [2] Hanany S, Alvarez M, Artis E, Ashton P, Aumont J, Aurlieu R, et al. PICO: Probe of Inflation and Cosmic Origins. *arXiv e-prints* (2019).
- [3] De Zotti G, Castex G, González-Nuevo J, Lopez-Caniego M, Negrello M, Cai ZY, et al. Extragalactic sources in Cosmic Microwave Background maps. *JCAP* **6** (2015) 018. doi:10.1088/1475-7516/2015/06/018.
- [4] Planck Collaboration III. Planck 2018 results. III. High Frequency Instrument data processing and frequency maps. *arXiv e-prints* (2018).
- [5] Mocanu LM, Crawford TM, Vieira JD, Aird KA, Aravena M, Austermann JE, et al. Extragalactic Millimeter-wave Point-source Catalog, Number Counts and Statistics from 771 deg² of the SPT-SZ Survey. *ApJ* **779** (2013) 61. doi:10.1088/0004-637X/779/1/61.
- [6] Delabrouille J, Betoule M, Melin JB, Miville-Deschênes MA, Gonzalez-Nuevo J, Le Jeune M, et al. The pre-launch Planck Sky Model: a model of sky emission at submillimetre to centimetre wavelengths. *A&A* **553** (2013) A96. doi:10.1051/0004-6361/201220019.
- [7] Chown R, Omori Y, Aylor K, Benson BA, Bleem LE, Carlstrom JE, et al. Maps of the Southern Millimeter-wave Sky from Combined 2500 deg² SPT-SZ and Planck Temperature Data. *ApJS* **239** (2018) 10. doi:10.3847/1538-4365/aae694.
- [8] González-Nuevo J, Argüeso F, López-Caniego M, Toffolatti L, Sanz JL, Vielva P, et al. The Mexican hat wavelet family: application to point-source detection in cosmic microwave background maps. *MNRAS* **369** (2006) 1603–1610. doi:10.1111/j.1365-2966.2006.10442.x.
- [9] López-Caniego M, Herranz D, González-Nuevo J, Sanz JL, Barreiro RB, Vielva P, et al. Comparison of filters for the detection of point sources in Planck simulations. *MNRAS* **370** (2006) 2047–2063. doi:10.1111/j.1365-2966.2006.10639.x.
- [10] Planck Collaboration XXVI. Planck 2015 results. XXVI. The Second Planck Catalogue of Compact Sources. *A&A* **594** (2016) A26. doi:10.1051/0004-6361/201526914.
- [11] De Zotti G, González-Nuevo J, Lopez-Caniego M, Negrello M, Greenslade J, Hernández-Monteaagudo C, et al. Exploring cosmic origins with CORE: Extragalactic sources in cosmic microwave background maps. *JCAP* **4** (2018) 020. doi:10.1088/1475-7516/2018/04/020.
- [12] Planck Collaboration XVIII. Planck early results. XVIII. The power spectrum of cosmic infrared background anisotropies. *A&A* **536** (2011) A18. doi:10.1051/0004-6361/201116461.
- [13] Planck Collaboration XXX. Planck 2013 results. XXX. Cosmic infrared background measurements and implications for star formation. *A&A* **571** (2014) A30. doi:10.1051/0004-6361/201322093.

- [14] Viero MP, Wang L, Zemcov M, Addison G, Amblard A, Arumugam V, et al. HerMES: Cosmic Infrared Background Anisotropies and the Clustering of Dusty Star-forming Galaxies. *ApJ* **772** (2013) 77. doi:10.1088/0004-637X/772/1/77.
- [15] Negrello M, Hopwood R, De Zotti Gea. The Detection of a Population of Submillimeter-Bright, Strongly Lensed Galaxies. *Science* **330** (2010) 800–. doi:10.1126/science.1193420.
- [16] Swinbank AM, Smail I, Longmore S, Harris AI, Baker AJ, De Breuck C, et al. Intense star formation within resolved compact regions in a galaxy at $z = 2.3$. *Nature* **464** (2010) 733–736. doi:10.1038/nature08880.
- [17] Combes F, Rex M, Rawle TD, Egami E, Boone F, Smail I, et al. A bright $z = 5.2$ lensed submillimeter galaxy in the field of Abell 773. HLSJ091828.6+514223. *A&A* **538** (2012) L4. doi:10.1051/0004-6361/201118750.
- [18] Zavala JA, Montaña A, Hughes DH, Yun MS, Ivison RJ, Valiante E, et al. A dusty star-forming galaxy at $z = 6$ revealed by strong gravitational lensing. *Nature Astronomy* **2** (2018) 56–62. doi:10.1038/s41550-017-0297-8.
- [19] Strandet ML, Weiss A, De Breuck C, Marrone DP, Vieira JD, Aravena M, et al. ISM Properties of a Massive Dusty Star-forming Galaxy Discovered at $z \sim 7$. *ApJL* **842** (2017) L15. doi:10.3847/2041-8213/aa74b0.
- [20] Marsden D, Gralla M, Marriage TA, Switzer ER, Partridge B, Massardi M, et al. The Atacama Cosmology Telescope: dusty star-forming galaxies and active galactic nuclei in the Southern survey. *MNRAS* **439** (2014) 1556–1574. doi:10.1093/mnras/stu001.
- [21] Abazajian KN, Adshead P, Ahmed Z, Allen SW, Alonso D, Arnold KS, et al. CMB-S4 Science Book, First Edition. *arXiv e-prints* (2016).
- [22] Ade P, Aguirre J, Ahmed Z, Aiola S, Ali A, Alonso D, et al. The Simons Observatory: science goals and forecasts. *JCAP* **2** (2019) 056. doi:10.1088/1475-7516/2019/02/056.
- [23] Planck Collaboration VI. Planck 2018 results. VI. Cosmological parameters. *arXiv e-prints* (2018).
- [24] Negrello M, Amber S, Amvrosiadis Aea. The Herschel-ATLAS: a sample of 500 μm -selected lensed galaxies over 600 deg^2 . *MNRAS* **465** (2017) 3558–3580. doi:10.1093/mnras/stw2911.
- [25] Cai ZY, Lapi A, Xia ea J-Q. A Hybrid Model for the Evolution of Galaxies and Active Galactic Nuclei in the Infrared. *ApJ* **768** (2013) 21. doi:10.1088/0004-637X/768/1/21.
- [26] Glenn J, Conley A, Béthermin M, Altieri B, Amblard A, Arumugam V, et al. HerMES: deep galaxy number counts from a P(D) fluctuation analysis of SPIRE Science Demonstration Phase observations. *MNRAS* **409** (2010) 109–121. doi:10.1111/j.1365-2966.2010.17781.x.
- [27] Tucci M, Toffolatti L, de Zotti G, Martínez-González E. High-frequency predictions for number counts and spectral properties of extragalactic radio sources. New evidence of a break at mm wavelengths in spectra of bright blazar sources. *A&A* **533** (2011) A57. doi:10.1051/0004-6361/201116972.
- [28] Vieira JD, Crawford TM, Switzer ER, Ade PAR, Aird KA, Ashby MLN, et al. Extragalactic Millimeter-wave Sources in South Pole Telescope Survey Data: Source Counts, Catalog, and Statistics for an 87 Square-degree Field. *ApJ* **719** (2010) 763–783. doi:10.1088/0004-637X/719/1/763.
- [29] Weiß A, De Breuck C, Marrone DP, Vieira JD, Aguirre JE, Aird KA, et al. ALMA Redshifts of Millimeter-selected Galaxies from the SPT Survey: The Redshift Distribution of Dusty Star-forming Galaxies. *ApJ* **767** (2013) 88. doi:10.1088/0004-637X/767/1/88.
- [30] Cañameras R, Nesvadba NPH, Guery ea D. Planck’s dusty GEMS: The brightest gravitationally lensed galaxies discovered with the Planck all-sky survey. *A&A* **581** (2015) A105. doi:10.1051/0004-6361/201425128.

- [31] González-Nuevo J, Lapi A, Fleuren S, Bressan S, Danese L, De Zotti G, et al. Herschel-ATLAS: Toward a Sample of ~1000 Strongly Lensed Galaxies. *ApJ* **749** (2012) 65. doi:10.1088/0004-637X/749/1/65.
- [32] González-Nuevo J, Suárez Gómez SL, Bonavera L, Sánchez-Lasheras F, Argüeso F, Toffolatti L, et al. SHALOS: Statistical Herschel-ATLAS Lensed Objects Selection. *arXiv e-prints* (2019).
- [33] Vieira JD, Marrone DP, Chapman SC, De Breuck C, Hezaveh YD, Weiß A, et al. Dusty starburst galaxies in the early Universe as revealed by gravitational lensing. *Nature* **495** (2013) 344–347. doi:10.1038/nature12001.
- [34] Su T, Marriage TA, Asboth V, Baker AJ, Bond JR, Crichton D, et al. On the redshift distribution and physical properties of ACT-selected DSFGs. *MNRAS* **464** (2017) 968–984. doi:10.1093/mnras/stw2334.
- [35] Crocker RM, Krumholz MR, Thompson TA, Clutterbuck J. The maximum flux of star-forming galaxies. *MNRAS* **478** (2018) 81–94. doi:10.1093/mnras/sty989.
- [36] Eales S, Dunne L, Clements D, Cooray A, De Zotti G, Dye S, et al. The Herschel ATLAS. *PASP* **122** (2010) 499. doi:10.1086/653086.
- [37] Negrello M, Hopwood R, Dye S, da Cunha E, Serjeant S, Fritz J, et al. Herschel *-ATLAS: deep HST/WFC3 imaging of strongly lensed submillimetre galaxies. *MNRAS* **440** (2014) 1999–2012. doi:10.1093/mnras/stu413.
- [38] Nayyeri H, Keele M, Cooray A, Riechers DA, Ivison RJ, Harris AI, et al. Candidate Gravitationally Lensed Dusty Star-forming Galaxies in the Herschel Wide Area Surveys. *ApJ* **823** (2016) 17. doi:10.3847/0004-637X/823/1/17.
- [39] Franceschini A, Toffolatti L, Mazzei P, Danese L, de Zotti G. Galaxy counts and contributions to the background radiation from 1 μm to 1000 μm . *A&A Supp.* **89** (1991) 285–310.
- [40] Blain AW, Longair MS. Submillimetre cosmology. *MNRAS* **264** (1993) 509–521. doi:10.1093/mnras/264.2.509.
- [41] York T, Jackson N, Browne IWA, Koopmans LVE, McKean JP, Norbury MA, et al. CLASS B0631+519: last of the Cosmic Lens All-Sky Survey lenses. *MNRAS* **361** (2005) 259–271. doi:10.1111/j.1365-2966.2005.09170.x.
- [42] Jackson N. Gravitational lenses and lens candidates identified from the COSMOS field. *MNRAS* **389** (2008) 1311–1318. doi:10.1111/j.1365-2966.2008.13629.x.
- [43] Treu T. Strong Lensing by Galaxies. *ARA&A* **48** (2010) 87–125. doi:10.1146/annurev-astro-081309-130924.
- [44] Negrello M, Perrotta F, González-Nuevo J. Astrophysical and cosmological information from large-scale submillimetre surveys of extragalactic sources. *MNRAS* **377** (2007) 1557–1568. doi:10.1111/j.1365-2966.2007.11708.x.
- [45] Jacobs C, Collett T, Glazebrook K, McCarthy C, Qin AK, Abbott TMC, et al. Finding high-redshift strong lenses in DES using convolutional neural networks. *MNRAS* **484** (2019) 5330–5349. doi:10.1093/mnras/stz272.
- [46] Serjeant S. Strong Gravitational Lenses and Multi-Wavelength Galaxy Surveys with Akari, Herschel, SPICA and EUCLID. *Publication of Korean Astronomical Society* **32** (2017) 251–255. doi:10.5303/PKAS.2017.32.1.251.
- [47] Silk J, Mamon GA. The current status of galaxy formation. *Research in Astronomy and Astrophysics* **12** (2012) 917–946. doi:10.1088/1674-4527/12/8/004.
- [48] Somerville RS, Davé R. Physical Models of Galaxy Formation in a Cosmological Framework. *ARA&A* **53** (2015) 51–113. doi:10.1146/annurev-astro-082812-140951.

- [49] Fujimoto S, Ouchi M, Kohno Kea. ALMA 26 Arcmin² Survey of GOODS-S at One Millimeter (ASAGAO): Average Morphology of High-*z* Dusty Star-forming Galaxies in an Exponential Disk ($n \simeq 1$). *ApJ* **861** (2018) 7. doi:10.3847/1538-4357/aac6c4.
- [50] Enia A, Negrello M, Gurwell M, Dye S, Rodighiero G, Massardi M, et al. The Herschel-ATLAS: magnifications and physical sizes of 500- μ m-selected strongly lensed galaxies. *MNRAS* **475** (2018) 3467–3484. doi:10.1093/mnras/sty021.
- [51] Cañameras R, Nesvadba N, Kneissl Rea. Planck’s dusty GEMS. IV. Star formation and feedback in a maximum starburst at $z = 3$ seen at 60-pc resolution. *A&A* **604** (2017) A117. doi:10.1051/0004-6361/201630186.
- [52] King A, Pounds K. Powerful Outflows and Feedback from Active Galactic Nuclei. *ARA&A* **53** (2015) 115–154. doi:10.1146/annurev-astro-082214-122316.
- [53] Ciccone C, Maiolino R, Gallerani S, Neri R, Ferrara A, Sturm E, et al. Very extended cold gas, star formation and outflows in the halo of a bright quasar at $z > 6$. *A&A* **574** (2015) A14. doi:10.1051/0004-6361/201424980.
- [54] Cresci G, Maiolino R. Observing positive and negative AGN feedback. *Nature Astronomy* **2** (2018) 179–180. doi:10.1038/s41550-018-0404-5.
- [55] Spilker JS, Aravena M, Béthermin Mea. Fast molecular outflow from a dusty star-forming galaxy in the early Universe. *Science* **361** (2018) 1016–1019. doi:10.1126/science.aap8900.
- [56] Cañameras R, Nesvadba NPH, Limousin M, Dole H, Kneissl R, Koenig S, et al. Planck’s dusty GEMS. V. Molecular wind and clump stability in a strongly lensed star-forming galaxy at $z = 2.2$. *A&A* **620** (2018) A60. doi:10.1051/0004-6361/201833679.
- [57] Spilker J, Nyland K. Characterizing Feedback Through Molecular Outflows Across Cosmic Time. Murphy E, editor, *Science with a Next Generation Very Large Array* (2018), *Astronomical Society of the Pacific Conference Series*, vol. 517, 657.
- [58] Leisawitz D, Amatucci E, Carter R, DiPirro M, Flores A, Staguhn J, et al. The Origins Space Telescope: mission concept overview. *Space Telescopes and Instrumentation 2018: Optical, Infrared, and Millimeter Wave* (2018), *Society of Photo-Optical Instrumentation Engineers (SPIE) Conference Series*, vol. 10698, 1069815. doi:10.1117/12.2313823.
- [59] Bonato M, De Zotti G, Leisawitz D, Negrello M, Massardi M, Baronchelli I, et al. Origins Space Telescope: Predictions for far-IR spectroscopic surveys. *PASA* **36** (2019) e017. doi:10.1017/pasa.2019.8.
- [60] Natarajan P, Sigurdsson S. Sunyaev–Zeldovich decrements with no clusters? *MNRAS* **302** (1999) 288–292. doi:10.1046/j.1365-8711.1999.02116.x.
- [61] Platania P, Burigana C, De Zotti G, Lazzaro E, Bersanelli M. Sunyaev-Zel’dovich effect from quasar-driven blast waves. *MNRAS* **337** (2002) 242–246. doi:10.1046/j.1365-8711.2002.05907.x.
- [62] Lacy M, Mason B, Sarazin C, Chatterjee S, Nyland K, Kimball A, et al. Direct detection of quasar feedback via the Sunyaev-Zeldovich effect. *MNRAS* **483** (2019) L22–L27. doi:10.1093/mnras/sly215.
- [63] Cañameras R, Nesvadba NPH, Kneissl Rea. Planck’s dusty GEMS. III. A massive lensing galaxy with a bottom-heavy stellar initial mass function at $z = 1.5$. *A&A* **600** (2017) L3. doi:10.1051/0004-6361/201630359.
- [64] Eales SA. Practical cosmology with lenses. *MNRAS* **446** (2015) 3224–3234. doi:10.1093/mnras/stu2214.
- [65] Li R, Frenk CS, Cole S, Gao L, Bose S, Hellwing WA. Constraints on the identity of the dark matter from strong gravitational lenses. *MNRAS* **460** (2016) 363–372. doi:10.1093/mnras/stw939.

- [66] Galvin TJ, Seymour N, Marvil J, Filipović MD, Tothill NFH, McDermid RM, et al. The spectral energy distribution of powerful starburst galaxies - I. Modelling the radio continuum. *MNRAS* **474** (2018) 779–799. doi:10.1093/mnras/stx2613.
- [67] Mancuso C, Lapi A, Cai ZY, Negrello M, De Zotti G, Bressan A, et al. Predictions for Ultra-deep Radio Counts of Star-forming Galaxies. *ApJ* **810** (2015) 72. doi:10.1088/0004-637X/810/1/72.
- [68] Aravena M, Murphy EJ, Aguirre JE, Ashby MLN, Benson BA, Bothwell M, et al. Large gas reservoirs and free-free emission in two lensed star-forming galaxies at $z = 2.7$. *MNRAS* **433** (2013) 498–505. doi:10.1093/mnras/stt741.
- [69] Planck Collaboration XLV. Planck intermediate results. XLV. Radio spectra of northern extragalactic radio sources. *A&A* **596** (2016) A106. doi:10.1051/0004-6361/201527780.
- [70] Ivison RJ, Swinbank AM, Smail I, Harris AI, Bussmann RS, Cooray A, et al. Herschel-ATLAS: A Binary HyLIRG Pinpointing a Cluster of Starbursting Protoellipticals. *ApJ* **772** (2013) 137. doi:10.1088/0004-637X/772/2/137.
- [71] Wang T, Elbaz D, Daddi E, Finoguenov A, Liu D, Schreiber C, et al. Discovery of a Galaxy Cluster with a Violently Starbursting Core at $z = 2.506$. *ApJ* **828** (2016) 56. doi:10.3847/0004-637X/828/1/56.
- [72] Miller TB, Chapman SC, Aravena M, Ashby MLN, Hayward CC, Vieira JD, et al. A massive core for a cluster of galaxies at a redshift of 4.3. *Nature* **556** (2018) 469–472. doi:10.1038/s41586-018-0025-2.
- [73] Oteo I, Ivison RJ, Dunne L, Manilla-Robles A, Maddox S, Lewis AJR, et al. An Extreme Protocluster of Luminous Dusty Starbursts in the Early Universe. *ApJ* **856** (2018) 72. doi:10.3847/1538-4357/aaaf1f.
- [74] Negrello M, Gonzalez-Nuevo J, De Zotti G. On the statistics of proto-cluster candidates detected in the Planck all-sky survey. *MNRAS* **470** (2017) 2253–2261. doi:10.1093/mnras/stx1367.
- [75] Bocquet S, Dietrich JP, Schrabback T, Bleem LE, Klein M, Allen SW, et al. Cluster Cosmology Constraints from the 2500 deg² SPT-SZ Survey: Inclusion of Weak Gravitational Lensing Data from Magellan and the Hubble Space Telescope. *arXiv e-prints* (2018).
- [76] Overzier RA. The realm of the galaxy protoclusters. A review. *A&A Rev.* **24** (2016) 14. doi:10.1007/s00159-016-0100-3.
- [77] Mehrrens N, Romer AK, Hilton M, Lloyd-Davies EJ, Miller CJ, Stanford SA, et al. The XMM Cluster Survey: optical analysis methodology and the first data release. *MNRAS* **423** (2012) 1024–1052. doi:10.1111/j.1365-2966.2012.20931.x.
- [78] Willis JP, Clerc N, Bremer MN, Pierre M, Adami C, Ilbert O, et al. Distant galaxy clusters in the XMM Large Scale Structure survey. *MNRAS* **430** (2013) 134–156. doi:10.1093/mnras/sts540.
- [79] Sunyaev RA, Zeldovich YB. The Observations of Relic Radiation as a Test of the Nature of X-Ray Radiation from the Clusters of Galaxies. *Comments on Astrophysics and Space Physics* **4** (1972) 173.
- [80] Bleem LE, Stalder B, de Haan T, Aird KA, Allen SW, Applegate DE, et al. Galaxy Clusters Discovered via the Sunyaev-Zel’dovich Effect in the 2500-Square-Degree SPT-SZ Survey. *ApJS* **216** (2015) 27. doi:10.1088/0067-0049/216/2/27.
- [81] Planck Collaboration XXVII. Planck 2015 results. XXVII. The second Planck catalogue of Sunyaev-Zeldovich sources. *A&A* **594** (2016) A27. doi:10.1051/0004-6361/201525823.
- [82] Hilton M, Hasselfield M, Sifón C, Battaglia N, Aiola S, Bharadwaj V, et al. The Atacama Cosmology Telescope: The Two-season ACTPol Sunyaev-Zeldovich Effect Selected Cluster Catalog. *ApJS* **235** (2018) 20. doi:10.3847/1538-4365/aaa6cb.

- [83] Rykoff ES, Rozo E, Hollowood D, Bermeo-Hernandez A, Jeltema T, Mayers J, et al. The RedMaPPer Galaxy Cluster Catalog From DES Science Verification Data. *ApJS* **224** (2016) 1. doi:10.3847/0067-0049/224/1/1.
- [84] Wen ZL, Han JL. A sample of 1959 massive galaxy clusters at high redshifts. *MNRAS* **481** (2018) 4158–4168. doi:10.1093/mnras/sty2533.
- [85] Gonzalez AH, Gettings DP, Brodwin M, Eisenhardt PRM, Stanford SA, Wylezalek D, et al. The Massive and Distant Clusters of WISE Survey. I. Survey Overview and a Catalog of > 2000 Galaxy Clusters at $z \simeq 1$. *ApJS* **240** (2019) 33. doi:10.3847/1538-4365/aafad2.
- [86] Maturi M, Bellagamba F, Radovich M, Roncarelli M, Sereno M, Moscardini L, et al. AMICO galaxy clusters in KiDS-DR3: sample properties and selection function. *MNRAS* **485** (2019) 498–512. doi:10.1093/mnras/stz294.
- [87] Dressler A. Galaxy morphology in rich clusters - Implications for the formation and evolution of galaxies. *ApJ* **236** (1980) 351–365. doi:10.1086/157753.
- [88] Alberts S, Pope A, Brodwin M, Atlee DW, Lin YT, Dey A, et al. The evolution of dust-obscured star formation activity in galaxy clusters relative to the field over the last 9 billion years. *MNRAS* **437** (2014) 437–457. doi:10.1093/mnras/stt1897.
- [89] Alberts S, Pope A, Brodwin M, Chung SM, Cybulski R, Dey A, et al. Star Formation and AGN Activity in Galaxy Clusters from $z=1-2$: a Multi-Wavelength Analysis Featuring Herschel/PACS. *ApJ* **825** (2016) 72. doi:10.3847/0004-637X/825/1/72.
- [90] Wagner CR, Courteau S, Brodwin Mea. The Evolution of Star formation Activity in Cluster Galaxies over $0.15 < z < 1.5$. *ApJ* **834** (2017) 53. doi:10.3847/1538-4357/834/1/53.
- [91] Planck Collaboration Int XXXIX. Planck intermediate results. XXXIX. The Planck list of high-redshift source candidates. *A&A* **596** (2016) A100. doi:10.1051/0004-6361/201527206.
- [92] Planck Collaboration Int XXVII. Planck intermediate results. XXVII. High-redshift infrared galaxy overdensity candidates and lensed sources discovered by Planck and confirmed by Herschel-SPIRE. *A&A* **582** (2015) A30. doi:10.1051/0004-6361/201424790.
- [93] Clements DL, Braglia FG, Hyde AKea. Herschel Multitiered Extragalactic Survey: clusters of dusty galaxies uncovered by Herschel and Planck. *MNRAS* **439** (2014) 1193–1211. doi:10.1093/mnras/stt2253.
- [94] Clements DL, Braglia F, Petitpas G, Greenslade J, Cooray A, Valiante E, et al. H-ATLAS: a candidate high redshift cluster/protocluster of star-forming galaxies. *MNRAS* **461** (2016) 1719–1733. doi:10.1093/mnras/stw1224.
- [95] Greenslade J, Clements DL, Cheng T, De Zotti G, Scott D, Valiante E, et al. Candidate high- z protoclusters among the Planck compact sources, as revealed by Herschel-SPIRE. *MNRAS* **476** (2018) 3336–3359. doi:10.1093/mnras/sty023.
- [96] Gómez-Guijarro C, Riechers DA, Pavesi R, Magdis GE, Leung TKD, Valentino F, et al. Confirming Herschel Candidate Protoclusters from ALMA/VLA CO Observations. *ApJ* **872** (2019) 117. doi:10.3847/1538-4357/ab002a.
- [97] Lacaille K, Chapman S, Smail I, Steidel C, Blain A, Geach J, et al. Two sub-millimetre bright protoclusters bounding the epoch of peak star formation activity. *arXiv e-prints* (2018).
- [98] Merloni A, Predehl P, Becker W, Böhringer H, Boller T, Brunner H, et al. eROSITA Science Book: Mapping the Structure of the Energetic Universe. *arXiv e-prints* (2012).
- [99] Melin JB, Bonaldi A, Remazeilles M, Hagstotz S, Diego JM, Hernández-Monteagudo C, et al. Exploring cosmic origins with CORE: Cluster science. *JCAP* **4** (2018) 019. doi:10.1088/1475-7516/2018/04/019.

- [100] Melin JB, Bartlett JG, Cai ZY, De Zotti G, Delabrouille J, Roman M, et al. Dust in galaxy clusters: Modeling at millimeter wavelengths and impact on Planck cluster cosmology. *A&A* **617** (2018) A75. doi:10.1051/0004-6361/201732292.
- [101] Planck Collaboration XIII. Planck early results. XIII. Statistical properties of extragalactic radio sources in the Planck Early Release Compact Source Catalogue. *A&A* **536** (2011) A13. doi:10.1051/0004-6361/201116471.
- [102] Bonato M, Liuzzo E, Herranz D, González-Nuevo J, Bonavera L, Tucci M, et al. ALMA photometry of extragalactic radio sources. *MNRAS* **485** (2019) 1188–1195. doi:10.1093/mnras/stz465.
- [103] Massardi M, Bonaldi A, Negrello M, Ricciardi S, Raccanelli A, de Zotti G. A model for the cosmological evolution of low-frequency radio sources. *MNRAS* **404** (2010) 532–544. doi:10.1111/j.1365-2966.2010.16305.x.
- [104] Rigby EE, Argyle J, Best PN, Rosario D, Röttgering HJA. Cosmic downsizing of powerful radio galaxies to low radio luminosities. *A&A* **581** (2015) A96. doi:10.1051/0004-6361/201526475.
- [105] Marscher AP, Gear WK. Models for high-frequency radio outbursts in extragalactic sources, with application to the early 1983 millimeter-to-infrared flare of 3C 273. *ApJ* **298** (1985) 114–127. doi:10.1086/163592.
- [106] Fuhrmann L, Angelakis E, Zensus JA, Nestoras I, Marchili N, Pavlidou V, et al. The F-GAMMA programme: multi-frequency study of active galactic nuclei in the Fermi era. Programme description and the first 2.5 years of monitoring. *A&A* **596** (2016) A45. doi:10.1051/0004-6361/201528034.
- [107] Fan XL, Wu Q. The Radio/Gamma Connection of Blazars from High to Low Radio Frequencies. *ApJ* **869** (2018) 133. doi:10.3847/1538-4357/aaeece.
- [108] Caccianiga A, Moretti A, Belladitta S, Della Ceca R, Antón S, Ballo L, et al. The space density of $z > 4$ blazars. *MNRAS* **484** (2019) 204–217. doi:10.1093/mnras/sty3526.
- [109] Ghisellini G, Nardini M, Tagliaferri G J, Schady P, Rau A, Foschini L, et al. High-redshift Fermi blazars observed by GROND and Swift. *MNRAS* **428** (2013) 1449–1459. doi:10.1093/mnras/sts140.
- [110] Ghisellini G, Tagliaferri G, Sbarrato T, Gehrels N. SDSS J013127.34 – 032100.1: a candidate blazar with an 11 billion solar mass black hole at $z = 5.18$. *MNRAS* **450** (2015) L34–L38. doi:10.1093/mnrasl/slv042.
- [111] De Zotti G, Ricci R, Mesa D, Silva L, Mazzotta P, Toffolatti L, et al. Predictions for high-frequency radio surveys of extragalactic sources. *A&A* **431** (2005) 893–903. doi:10.1051/0004-6361:20042108.
- [112] Lähteenmäki A, Järvelä E, Ramakrishnan V, Tornikoski M, Tammi J, Vera RJC, et al. Radio jets and gamma-ray emission in radio-silent narrow-line Seyfert 1 galaxies. *A&A* **614** (2018) L1. doi:10.1051/0004-6361/201833378.
- [113] Bruni G, Panessa F, Bassani L, Chiaraluze E, Kraus A, Dallacasa D, et al. A Discovery of Young Radio Sources in the Cores of Giant Radio Galaxies Selected at Hard X-Rays. *ApJ* **875** (2019) 88. doi:10.3847/1538-4357/ab1006.
- [114] Doi A, Kamenno S, Kohno K, Nakanishi K, Inoue M. A high-frequency radio survey of low-luminosity active galactic nuclei. *MNRAS* **363** (2005) 692–704. doi:10.1111/j.1365-2966.2005.09471.x.
- [115] Tinti S, De Zotti G. Constraints on evolutionary properties of GHz Peaked Spectrum galaxies. *A&A* **445** (2006) 889–899. doi:10.1051/0004-6361:20053752.
- [116] Blandford RD, McKee CF. Fluid dynamics of relativistic blast waves. *Physics of Fluids* **19** (1976) 1130–1138. doi:10.1063/1.861619.
- [117] Granot J, Sari R. The Shape of Spectral Breaks in Gamma-Ray Burst Afterglows. *ApJ* **568** (2002) 820–829. doi:10.1086/338966.

- [118] Metzger BD, Williams PKG, Berger E. Extragalactic Synchrotron Transients in the Era of Wide-field Radio Surveys. I. Detection Rates and Light Curve Characteristics. *ApJ* **806** (2015) 224. doi:10.1088/0004-637X/806/2/224.
- [119] Whitehorn N, Natoli T, Ade PAR, Austermann JE, Beall JA, Bender AN, et al. Millimeter Transient Point Sources in the SPTpol 100 Square Degree Survey. *ApJ* **830** (2016) 143. doi:10.3847/0004-637X/830/2/143.
- [120] Ho AYQ, Phinney ES, Ravi V, Kulkarni SR, Petitpas G, Emonts B, et al. AT2018cow: A Luminous Millimeter Transient. *ApJ* **871** (2019) 73. doi:10.3847/1538-4357/aaf473.
- [121] Remazeilles M, Banday AJ, Baccigalupi C, Basak S, Bonaldi A, De Zotti G, et al. Exploring cosmic origins with CORE: B-mode component separation. *JCAP* **4** (2018) 023. doi:10.1088/1475-7516/2018/04/023.
- [122] Battye RA, Browne IWA, Peel MW, Jackson NJ, Dickinson C. Statistical properties of polarized radio sources at high frequency and their impact on cosmic microwave background polarization measurements. *MNRAS* **413** (2011) 132–148. doi:10.1111/j.1365-2966.2010.18115.x.
- [123] Galluzzi V, Massardi M, Bonaldi A, Casasola V, Gregorini L, Trombetti T, et al. Characterization of polarimetric and total intensity behaviour of a complete sample of PACO radio sources in the radio bands. *MNRAS* **475** (2018) 1306–1322. doi:10.1093/mnras/stx3216.
- [124] Galluzzi V, Puglisi G, Burkutean S, Liuzzo E, Bonato M, Massardi M, et al. ALMA Band 3 polarimetric follow-up of a complete sample of faint PACO sources. *arXiv e-prints* (2019) arXiv:1907.00299.
- [125] Datta R, Aiola S, Choi SK, Devlin M, Dunkley J, Dünner R, et al. The Atacama Cosmology Telescope: two-season ACTPol extragalactic point sources and their polarization properties. *MNRAS* **486** (2019) 5239–5262. doi:10.1093/mnras/sty2934.
- [126] Gupta N, Reichardt CL, Ade PAR, Anderson AJ, Archipley M, Austermann JE, et al. Fractional Polarisation of Extragalactic Sources in the 500-square-degree SPTpol Survey. *arXiv e-prints* (2019) arXiv:1907.02156.
- [127] Bonavera L, González-Nuevo J, Argüeso F, Toffolatti L. Statistics of the fractional polarization of compact radio sources in Planck maps. *MNRAS* **469** (2017) 2401–2411. doi:10.1093/mnras/stx1020.
- [128] Trombetti T, Burigana C, De Zotti G, Galluzzi V, Massardi M. Average fractional polarization of extragalactic sources at Planck frequencies. *A&A* **618** (2018) A29. doi:10.1051/0004-6361/201732342.
- [129] Greaves JS, Holland WS. Submillimetre polarization of M82 and the Galactic Center: Implications for CMB polarimetry. Cecchini S, Cortiglioni S, Sault R, Sbarra C, editors, *Astrophysical Polarized Backgrounds* (2002), *American Institute of Physics Conference Series*, vol. 609, 267–270. doi:10.1063/1.1471859.
- [130] Seiffert M, Borys C, Scott D, Halpern M. An upper limit to polarized submillimetre emission in Arp 220. *MNRAS* **374** (2007) 409–414. doi:10.1111/j.1365-2966.2006.11186.x.
- [131] Bonavera L, González-Nuevo J, De Marco B, Argüeso F, Toffolatti L. Statistics of the fractional polarization of extragalactic dusty sources in Planck HFI maps. *MNRAS* **472** (2017) 628–635. doi:10.1093/mnras/stx2102.
- [132] Nartallo R, Gear WK, Murray AG, Robson EI, Hough JH. A Millimetre/Submillimetre Polarization Survey of Compact Flat-Spectrum Radio Sources. *MNRAS* **297** (1998) 667–686. doi:10.1046/j.1365-8711.1998.01405.x.
- [133] Saikia DJ, Salter CJ. Polarization properties of extragalactic radio sources. *ARA&A* **26** (1988) 93–144. doi:10.1146/annurev.aa.26.090188.000521.